

Stochastic optimal control of open quantum systems

Aarón Villanueva and Hilbert Kappen

Radboud University, Heyendaalseweg 135, 6525 AJ Nijmegen, The Netherlands

We address the generic problem of optimal quantum state preparation for open quantum systems. It is well known that open quantum systems can be simulated by quantum trajectories described by a stochastic Schrödinger equation. In this context, the state preparation becomes a stochastic optimal control (SOC) problem. The latter requires the solution of the Hamilton-Jacobi-Bellman equation, which is, in general, challenging to solve. A notable exception are the so-called path integral (PI) control problems, for which one can estimate the optimal control solution by direct sampling of the cost objective. In this work, we derive a class of quantum state preparation problems that are amenable to PI control techniques, and propose a corresponding algorithm, which we call Quantum Diffusion Control (QDC). Unlike conventional quantum control algorithms, QDC avoids computing gradients of the cost function to determine the optimal control. Instead, it employs adaptive importance sampling, a technique where the controls are iteratively improved based on global averages over quantum trajectories. We also demonstrate that QDC, used as an annealer in the environmental coupling strength, finds high accuracy solutions for unitary (noiseless) quantum control problems. We further discuss the implementation of this technique on quantum hardware. We illustrate the effectiveness of our approach through examples of open-loop control for single- and multi-qubit systems.

1 Introduction

Effectively and efficiently controlling quantum systems to achieve desired behaviors has wide-ranging applications, including quantum error correction [1], quantum simulation [2], quantum metrology [3], quantum sensing [4], state preparation [5], quantum state transfer [6], and quantum gate synthesis [7]. Recent advancements in experimental capabilities for measuring and manipulating quantum systems at the atomic, molecular, and optical levels [8–12] have further fueled the development of efficient and scalable quantum control techniques [13, 14].

Open-loop quantum optimal control (QOC) involves state-independent controls that depend solely on time [15, 16]. In the unitary case, open-loop QOC problems [17] have been tackled with various methods, including the gradient-based GRAPE algorithm [18] and its variants [19], search-based methods such as CRAB [20], variational approaches like Krotov optimization [21–24], and techniques derived from the Pontryagin Maximum Principle (PMP) [25]. These methods have been successfully applied to a broad range of quantum control tasks [13, 14].

The control of open quantum systems has also been a topic of intense research [14, 26]. Methods based on master equations, such as the Lindblad equation [27–29], become computationally demanding as the system size n grows, since they require evolving density matrices rather than wave functions. Furthermore, gradient-based methods rely on local optimization. In some cases, the gradients can be computed analytically or numerically [29]. In others, the gradients can only be computed approximately, relying on suitable truncations of series expansions; an example is k -order Open GRAPE [27].

Aarón Villanueva: aaronv@science.ru.nl
Hilbert Kappen: b.kappen@science.ru.nl

On the other hand, the theory of stochastic *quantum trajectories* [30–33] have constituted a useful framework for simulating open system dynamics in presence or absence of measurement, and has found numerous applications [34–40]. In coherent control of open systems, in particular, quantum trajectories have been used for to compute gradients, benefiting from the quadratic scaling advantage of propagating wave functions of size $N = 2^n$, over density matrices of size N^2 [41]. However, this approach still relies on estimating gradient approximations.

Quantum trajectories can be formulated using stochastic Schrödinger equations (SSEs) [32, 42, 43], often modeled as Brownian diffusions. The coherent control of open quantum systems via SSEs intrinsically leads to a stochastic optimal control (SOC) problem [44–46], as reviewed in [47]. Solving SOC problems generally involves tackling the Bellman equation or a stochastic variant of the PMP via backward stochastic differential equations [48, 49], both of which may pose significant computational challenges. A notable exception are linear-quadratic-Gaussian (LQG) problems, where the dynamics are linear, the cost is quadratic in the control, and the noise is additive and Gaussian. While SSEs with coherent controls are not in LQG form due to the bilinearity introduced by terms such as $u\psi$, certain cases admit LQG formulations in the Heisenberg picture [47], enabling applications in feedback control [9, 12, 50, 51]. In general, however, the control of open quantum systems governed by SSEs is a nonlinear control problem, for which no efficient solution method has been widely available.

The path integral (PI) control method was proposed in [52–54] to efficiently solve a large class of non-linear SOC problems, for which LQG is a special case. This class includes problems with nonlinear dynamics, Gaussian noise, and nonlinear control cost. The key advantage of PI formulation is that the optimal control solution can be expressed in closed form as a path integral, circumventing the need to solve the Bellman or PMP equations. The path integral can be computed through direct sampling, which is further optimized using adaptive importance sampling (IS) [53]. IS enables the computation of statistics based on self-generated trajectories, making the method highly parallelizable with minimal computational overhead. PI control has demonstrated remarkable success in robotics, enabling solutions to high-dimensional, nonlinear problems with real-time constraints where traditional methods often fail [55]. For a recent review on PI control and related advances, see [56].

1.1 Contributions

In this work we propose a novel approach for coherent QOC of open systems, by formulating the problem as a SOC problem and leveraging PI control techniques to derive closed-form expressions for the optimal controls. Specifically, we focus on pulse-based control of the Lindblad equation. We simulate the Lindblad dynamics using a class of SSEs that can be formulated in PI form. We provide explicit expressions for the optimal control pulses u_k^* as weighted averages over quantum trajectories. We outline the general formula as (see (17))

$$u_k^* = u_k + \left\langle \omega^u \frac{\Delta W_k}{\Delta t_k} \right\rangle_u$$

where u is an arbitrary pulse sequence (the control sampler), ω^u is a weight associated with a u -controlled trajectory, and $\frac{\Delta W_k}{\Delta t_k}$ is the slope of the Wiener noise accumulated in the k -th time interval. The expectation $\langle \cdot \rangle_u$ is taken over all u -controlled quantum trajectories and constitutes a global quantity. This distinguishes our approach from local methods, as it does not rely on gradient computations.

A key property of this formula is its validity for any choice of control sampler u . However, the accuracy of estimating the optimal pulses u^* depends critically on the choice of the sampler. To address this, we employ adaptive importance sampling, iteratively refining the sampler to improve the estimation of u^* .

The resulting method, which we call Quantum Diffusion Control (QDC), constitute a new framework for computing optimal controls for a wide range of quantum control problems [57]. Unlike conventional approaches that rely on local gradients/finite differences, QDC iteratively improves global estimations through adaptive sampling.

Furthermore, we propose to use QDC as a quantum control annealer to compute optimal controls for unitary dynamics. In QDC, the environment enters the control optimization in form of dissipative coupling terms in the Lindblad equation. We propose using dissipation to design annealing control protocols, in which we start the optimization with large dissipation and gradually reduce it to approach the closed-system dynamics. The dissipation operators compatible with PI control constitute a subspace, offering substantial flexibility in the design of annealing protocols. We test this technique on Nuclear Magnetic Resonance (NMR) systems, finding excellent controls for the unitary case. We believe this approach offers a promising research direction towards noise-engineered quantum control.

To the best of our knowledge, this work represents the first attempt to integrate state-centered quantum trajectories with PI control techniques as introduced in [52–54]. Additionally, we argue that this framework has the potential to be extended to measurement-based control, as PI control theory inherently provides optimal feedback controls in the idealized scenario where the quantum state ψ is directly observable.

The rest of the paper is organized as follows. In Section 2, we provide the necessary background knowledge of continuous-time unravelings of the Lindblad equation. In Section 2.1, we define a class of transformations on the Lindblad operators and the noise matrix that leaves the Lindblad equation invariant while changing the unraveling. This transformation proves instrumental for mapping many interesting control problems originally formulated in Lindblad form onto stochastic optimal control problems of the PI form. In Section 3, we review the main results from path integral control theory. The optimal control that results from solving the path integral equations is a feedback control, i.e. it depends on the system state. In practice, computing the optimal control exactly can be challenging if not unfeasible due to the infinite dimensionality of the control. In Section 3.1, we use an importance sampling scheme to approximate the optimal control by a surrogate model based on linear combinations of arbitrary basis functions. In Section 4, we present our quantum control algorithm by combining quantum unravelings with path integral control. In Section 6, we show some proof-of-principle numerical examples of state preparation. In Section 6.1 we apply QDC to a single qubit. We show QDC’s robustness in finding global solutions while avoiding local minima, and compare this with OpenGRAPE. In Section 6.2, we show that finite-temperature QDC solutions can be used as proxy controls for the corresponding unitary problem. In Section 6.3 we apply QDC to NMR systems, developing the formalism for the general case and demonstrating it on a 4-qubit example. Additionally, we use annealing QDC to solve the corresponding unitary control problem, achieving several orders of magnitude improvement in infidelity compared to the literature using GRAPE. In Sections 7 and 8, we close with discussions about the challenges and prospects of future work.

2 Unravelings of the Lindblad equation

Consider the Lindblad equation [58]¹

$$\dot{\rho} = -i[H, \rho] + \mathcal{D}[D, C]\rho \quad \mathcal{D}[D, C]\rho := D_{ab} \left(C_a \rho C_b^\dagger - \frac{1}{2} \{C_b^\dagger C_a, \rho\} \right) \quad (1)$$

where \mathcal{D} denotes the dissipation superoperator, H is the system’s Hamiltonian, and C_a ($a = 1, \dots, n_c$) are the Lindblad operators. The noise matrix D is assumed to be positive semidefinite. This is a sufficient condition, although not necessary [59], for ensuring positive evolution maps. In this study, we restrict D to be real symmetric.

Equation (39) can be obtained as an average dynamics over all particular time realizations of a stochastic quantum state ψ_t . This leads to the theory of stochastic quantum unravelings [60]. The mathematical framework behind this theory was formulated by [46, 61–63]. Stochastic unravelings for non-Markovian scenarios can be traced back to Diosi [64] and Wiseman [65]. Quantum unravelings are usually encoded as stochastic differential equations (SDEs) of the state ψ_t . The SDE is designed in such

¹Along the text, repeated indices denote summation convention unless we explicitly state the contrary.

a way that the density operator $P = \psi_t \psi_t^\dagger$ follows in average a Lindblad evolution, i.e. $\rho = \langle \psi_t \psi_t^\dagger \rangle$, with ρ satisfying (39). One can define unravelings in many ways, for instance using stochastic jumps at discrete times, or using continuous Wiener noise. In this work we use the latter. Assume the following stochastic Schrödinger equation

$$d\psi = -iH\psi dt - \frac{1}{2}D_{ab} \left(C_b^\dagger C_a - 2c_a C_b + c_a c_b \right) \psi dt + (C_a - c_a)\psi dW_a \quad (2)$$

with dW_a a real-valued Wiener process with $\langle dW_a \rangle = 0$ and $\langle dW_a dW_b \rangle = D_{ab} dt$, with D a symmetric matrix. For notational ease we omit, when convenient, the time subscript from stochastic variables. The C_a are the Lindblad operators appearing in (39) and $c_a := \psi^\dagger C_a^{(h)} \psi$ with $C_a^{(h)} := \frac{1}{2} (C_a + C_a^\dagger)$, the Hermitian part of C_a . Given these definitions, one can state the following result.

Proposition 1. *Eq. (2) is an unraveling of the Lindblad equation (39).*

The proof is straightforward using Ito calculus, and we remit the reader to the Supplementary Material. See also [32, 47, 66, 67] for previous derivations of this result. The specific form of (2) is not arbitrary, and its derivation satisfies very general physical constraints. If one considers that the term $C_a \psi dW_a$ in (2) implements the basic stochastic action from the environment onto the quantum state, then the remaining terms are needed to ensure ψ normalization ($d\|\psi\|^2 = 0$). The c_a terms introduce non-linearities in the dynamics. This is a natural consequence of the stochastic non-Hermitian interaction of the system with the environment, which makes the evolution non-unitary and, therefore, violates norm preservation. A non-unitary norm preserving dynamics is necessarily non-linear.

2.1 Invariance of the Lindblad equation

Consider the Lindblad equation (39), where we assume the C_a to be linearly independent. They span a n_c -dimensional space of operators \mathcal{S} and the C_a form a (generally non-orthogonal) basis for \mathcal{S} . Given an $n_c \times n_c$ invertible complex-valued matrix A , define the following linear transformation on the Lindblad operators C_a and the noise matrix D ,

$$\tilde{C}_b = C_a A_{ab} \quad D = A \tilde{D} A^\dagger \quad (3)$$

This linear transformation leaves the dissipation operator (and, therefore, the Lindblad equation (39)) $\mathcal{D}[D, C]$ invariant

$$\mathcal{D}[D, C] = \mathcal{D}[\tilde{D}, \tilde{C}]. \quad (4)$$

On the other hand, transformation (3) changes the form of the SSE (2). Thus, the gauge freedom induced by transformation (3) gives rise to an infinite class of different but equivalent quantum unravelings simulating the same Lindblad equation. Obviously, this freedom allows for the design of different unravelings that can be more or less convenient depending on the problem we want to solve. In particular, if we can find a transformation A that leaves \tilde{C}_a ($a = 1, \dots, n_c$) anti-Hermitian and \tilde{D} real symmetric, then the non-linear terms $\tilde{c}_a = \psi^\dagger \tilde{C}_a^{(h)} \psi = 0$, and *the unraveling of the Lindblad equation in terms of the \tilde{C}_a and \tilde{D} is both linear and norm-preserving*:

$$d\psi = -iH\psi dt - \frac{1}{2}\tilde{D}_{ab}\tilde{C}_b^\dagger\tilde{C}_a\psi dt + \tilde{C}_a\psi d\tilde{W}_a \quad \langle d\tilde{W}_a d\tilde{W}_b \rangle = \tilde{D}_{ab} dt \quad (5)$$

For instance, when all C_a are Hermitian, the unraveling (2) is non-linear with $c_a = \psi^\dagger C_a \psi$. Using (3) with $A_{ab} = i\delta_{ab}$ gives $\tilde{C}_a = iC_a$ anti-Hermitian and $\tilde{D} = D$, and the unraveling is linear.

The transformation to a basis of anti-Hermitian operators is clearly not always possible. A necessary condition is that the space \mathcal{S} must contain anti-Hermitian operators. Take the case $n_c = 1$, where C_1 is neither Hermitian nor anti-Hermitian. The operator \tilde{C}_1 cannot be made anti-Hermitian for any A . For a non-trivial example, see Section 6.1.

As we will see in the following Sections, the transformation to anti-Hermitian operators turns out to be essential to cast the control of the unravelings as a path integral control problem. The fact that the unravelings also become linear in this case is a complimentary bonus.

3 The path integral control method

We briefly review the path integral control theory [52] in its most general form. See [54] for details. Consider a dynamical system of the form

$$dX_t^u = f(t, X_t^u)dt + g(t, X_t^u)(u(t, X_t^u)dt + dW_t) \quad (6)$$

for $t_0 \leq t \leq T$ with X_t^u an n -dimensional real stochastic variable, with initial condition $X_{t_0}^u = x_0$. Here W_t is a n_c -dimensional real Brownian motion with $\langle dW_t^a \rangle = 0$ and $\langle dW_t^a dW_t^b \rangle = \nu^{ab}dt$ with ν a $n_c \times n_c$ positive symmetric matrix. We take $f : [t_0, T] \times \mathbb{R}^n \rightarrow \mathbb{R}^n$, $g : [t_0, T] \times \mathbb{R}^n \rightarrow \mathbb{R}^{n \times n_c}$ and $u : [t_0, T] \times \mathbb{R}^n \rightarrow \mathbb{R}^{n_c}$. Given the function $u(t, x)$ that defines the control for each state x and each time t , we define the cost ²

$$S^u(t) = \Phi(X_T^u) + \int_t^T \left[V(s, X_s^u)ds + \frac{1}{2}u(s, X_s^u)^T R u(s, X_s^u)ds + u(s, X_s^u)^T R dW_s \right] \quad (7)$$

with X_t^u the stochastic solution of (20) at time t . The matrix R is positive $n_c \times n_c$ symmetric such that $R = \lambda \nu^{-1}$ with $\lambda > 0$ a constant. The function V is the state-dependent path cost and Φ the end cost. The control problem is to find the function u that minimizes

$$J(t_0, x_0) = \min_u \langle S^u(t_0) \rangle \quad (8)$$

where $\langle \cdot \rangle$ denotes the average over all possible realizations $X_{t_0:T}^u$ conditioned on $X_{t_0}^u = x_0$. The function $u^* : [t_0, T] \times \mathbb{R}^n \rightarrow \mathbb{R}^{n_c}$ that minimizes (8) is called the optimal control.

The generic approach to solve a stochastic optimal control problem is to derive a partial differential equation for $J(t, x)$, known as the Bellman equation, from which one computes the optimal control (see proof of Lemma 1 in the Supplementary Material). For the class of control problems defined above, one can establish the following result.

Theorem 1. *The optimal cost-to-go and optimal control of the control problem with dynamics (6) and cost (7) and (8) is given by*

$$J(t_0, x_0) = -\lambda \log \langle e^{-S^u(t_0)/\lambda} \rangle \quad (9)$$

$$\hat{u}(t_0, x_0) = u(t_0, x_0) + \lim_{dt \rightarrow 0} \left\langle \omega^u \frac{W_{t_0+dt}}{dt} \right\rangle \quad (10)$$

where $\omega^u := \frac{e^{-S^u(t_0)/\lambda}}{\langle e^{-S^u(t_0)/\lambda} \rangle}$.

Proof. The proof is given in [54] and reproduced in the Supplementary Material. Equation (9) follows directly from Corollary 2 of the Supplementary Material by taking $t = t_0$, and the proof of (9) is established in Corollary 4 of the Supplementary Material. \square

Theorem 1 gives an explicit solution of the optimal cost-to-go and optimal control at t_0, x_0 in terms of path integrals. Therefore the optimal control solution can be obtained by sampling. The control function u is referred to as the sampling control. Note that the l.h.s. of Eqs. (9) and (9) are independent of u : The result holds for any sampling control u , for instance the naive sampling control $u(x, t) = 0$. However, naive sampling strategies yield estimates with large statistical variance.

In Eqs. (9) and (9), the cost of the i -th sample trajectory is given by $S_i^u(t_0)$. Each trajectory is weighted by $\omega_i = \frac{e^{-S_i^u(t_0)/\lambda}}{\sum_{j=1}^{N_{traj}} e^{-S_j^u(t_0)/\lambda}}$, with N_{traj} the total number of trajectories. When $S_i^u(t_0)$ has large variance, the batch of samples is dominated by one sample: the sample with lowest $S_i^u(t_0)$, in

²Note, that the expectation of the last term in (7) vanishes, but this term is needed later when deriving the optimal solution of the path integral theory.

particular for low λ (i.e. low noise). The quality of the sampling can be quantified by the effective sample size [54]

$$ESS := N_{\text{eff}}/N_{\text{traj}}, \quad N_{\text{eff}} := \left(\sum_{i=1}^{N_{\text{traj}}} w_i^2 \right)^{-1} \quad (11)$$

where $1/N_{\text{traj}} \leq ESS \leq 1$ and reaches its maximal value $ESS = 1$ when $N_{\text{eff}} = N_{\text{traj}}$ with all samples having equal weight $w_i = 1/N_{\text{traj}}$. In [54], it was shown that sampling controls with lower control cost (8) are better samplers in the sense of smaller statistical variance and larger ESS . The optimal sampling control is given by the optimal control solution with minimal cost of J in (8): When u is the optimal control solution, the variance of $S^u(t_0)$ is zero, $w_i = 1/N_{\text{traj}}$ and $ESS = 1$. Thus any u implements an importance sampler, that is, an unbiased estimator of J and \hat{u} , but with different quality in terms of statistical variance. This is the basic idea of adaptive importance sampling, discussed in Section 3.1.

The quality of the control solution is in principle given by the value of the control cost J in (8). Because of the monotonic relation between control cost and effective sample size, one can also measure the quality of the control solution in terms of ESS instead of J , which turns out to be a more sensitive measure of optimality.

3.1 Adaptive importance sampling

In practice, the optimal control must be estimated at all spacetime points (t, x) , not just at the initial conditions (t_0, x_0) . For this, it is useful to parametrize the control functions \hat{u} and u . We consider linear parametrizations

$$\hat{u}_a(t, x) = \sum_{k \in I} \hat{A}_{ak} h_k(t, x), \quad u_a(t, x) = \sum_{k \in I} A_{ak} h_k(t, x) \quad a = 1, \dots, n_c \quad (12)$$

where \hat{A}_{ak}, A_{ak} are constants and $h_k : [t_0, T] \times \mathbb{R}^n \rightarrow \mathbb{R}$ are fixed basis functions. The symbol I denotes the index set labeling the basis functions.

Using Theorem 3 (Supp. Material) with $f(t, x) = h_{k'}(t, x)$ we obtain the following matrix equation

$$\sum_k (\hat{A}_{ak} - A_{ak}) B_{kk'} = C_{ak'} \quad (13)$$

with

$$B_{kk'} = \left\langle e^{-S^u(t_0)/\lambda} \int_{t_0}^T h_k(t, X_t^u) h_{k'}(t, X_t^u) dt \right\rangle \quad C_{ak} = \left\langle e^{-S^u(t_0)/\lambda} \int_{t_0}^T h_k(t, X_t^u) dW_t^a \right\rangle \quad (14)$$

We remark that this equation can also be obtained by minimizing the KL divergence between the distributions generated by the optimal solution and the parametrized model, respectively [53].

The statistics $B_{k_1 k_2}$ and C_{ak} can be estimated simultaneously using one batch of sample trajectories. Eq. (13) can be solved for the matrix \hat{A} in terms of the matrices A, B and C by matrix inversion:

$$\hat{A} = A + CB^{-1} \quad (15)$$

Eq. (15) gives an approximation to the optimal feedback control solution in terms of the sampling control A and the expectations B, C , which are estimated by sampling, with sampling control u .

One can iteratively apply (15) using the \hat{A} that is computed at iteration p as the sampler for iteration $p + 1$. This is called adaptive importance sampling and (15) takes the form

$$A^{p+1} = A^p + C^p (B^p)^{-1} \quad (16)$$

The procedure can be initialized for instance with $A_0 = 0$ or any other value³.

In particular, a piece-wise constant open-loop control ($u_a(t, x) = u_a(t)$) is obtained as follows. Consider the K intervals $I_k = [\tau_{k-1}, \tau_k]$ with time points $t_0 = \tau_0, \tau_1, \dots, \tau_K = T$. Define h_k in (12) as the indicator functions $h_k(t) = \delta_{t \in I_k}$. The adaptive importance sampling equation becomes

$$A_{ak}^{p+1} = A_{ak}^p + \left\langle \omega_p^u \frac{\Delta W_k^a}{\Delta \tau_k} \right\rangle_p \quad k = 1, \dots, K \quad (17)$$

where $\omega_p^u := \frac{e^{-S^u(t_0)/\lambda}}{\langle e^{-S^u(t_0)/\lambda} \rangle_p}$, $\Delta W_k^a := \int_{I_k} dW_t^a$, $\Delta \tau_k := \tau_k - \tau_{k-1}$, and $\langle \cdot \rangle_p$ denotes the statistics computed with control A^p .

From our numerical experiments we find that the adaptive importance sampling finds better solutions when a form of smoothing is introduced: we replace A_{ak}^p on the right hand side of (17) (in both terms) by a recent average over a window of past IS steps: $\frac{1}{w} \sum_{p'=p-w+1}^p A_{ak}^{p'}$ with w the window size. However, smoothing results in a slower convergence of the algorithm.

4 Path integral control of open quantum systems

We now consider the state preparation problem. We want to prepare a quantum state from a given initial state in total time T , taking into account the interactions between system and environment. For this, we assume the system dynamics follows the Lindblad equation (39). One can formulate this as a finite horizon control problem, where the Hamiltonian in (39) takes the form $H = H_0 + u_a H_a$ with $H_a (a = 1, \dots, n_c)$ a set of Hermitian operators and $u_a (a = 1, \dots, n_c)$ real-valued control fields. Given the time interval $[0, T]$, we consider the control objective

$$C[u] = -\frac{Q}{2} \mathcal{F}(\rho_T) + \frac{1}{2} \int_0^T u_t^T R u_t dt \quad (18)$$

where ρ_T represents the quantum state at the final time T , Q is a positive constant and R is a real symmetric positive $n_c \times n_c$ matrix. The objective is composed of two parts. The first term is the fidelity $\mathcal{F}(\rho_T) = \text{Tr}(\rho_T \phi \phi^\dagger)$ of the final state ρ_T with respect to a target (pure) state ϕ . The second term is an energy constraint, and it penalizes the accumulated magnitude of the different controls. We want to find the optimal open-loop control u^* that minimizes the objective function (18):

$$u^* = \underset{u}{\text{argmin}} C[u]$$

The Lindblad equation (39) and the cost (18) define a deterministic control problem. It can be approached by using, for example, the PMP method [25]. Here instead, we propose to address this problem as a SOC problem based on unravelings of the Lindblad equation. For this, consider instead the cost functional

$$C = \left\langle -\frac{Q}{2} \mathcal{F}(\psi_T) + \frac{1}{2} \int_0^T u_t^T R u_t dt \right\rangle \quad (19)$$

where ψ_t is the quantum state satisfying the SSE (2) and $\mathcal{F}(\psi) = \text{Tr}(\psi \psi^\dagger \phi \phi^\dagger)$. When the controls depend on the state, the problem is referred to as closed-loop/feedback control. These control problems can be solved using the PI control formalism when the Lindblad operators C_a can be transformed into anti-Hermitian operators $-iH_a$ using the transformation (3), while maintaining a real symmetric covariance matrix, as discussed in Sec. 2.1. When the transformation is possible, the unraveling is linear and norm-preserving, and the SSE takes the form

$$d\psi = -iH_0\psi dt - \frac{1}{2} \tilde{D}_{ab} H_a H_b \psi dt - iH_a \psi (u_a dt + d\tilde{W}_a) \quad \left\langle d\tilde{W}_a d\tilde{W}_b \right\rangle = \tilde{D}_{ab} dt \quad (20)$$

³For instance, with the solution of the corresponding deterministic control solution ($D = 0$) that can be efficiently obtained using PMP or GRAPE.

In addition, the transformation should leave the cost (19) invariant. The first term is invariant because $\langle \text{Tr}(\psi_T \psi_T^\dagger Q) \rangle = \text{Tr}(\rho_T Q)$ and ρ_T is invariant. The second term is generally not invariant, except when u is open-loop. For feedback control, the stochastic optimal control formulation depends on the specific unraveling employed.

The control problem defined by Eqs. (20) and (19) is in path integral form ⁴, as discussed in Section 3, provided that $R\tilde{D} = \lambda I$ with I denoting the identity matrix, and $\lambda > 0$. The open-loop control solution can therefore be estimated using the adaptive importance sampling approach given by (17). We refer to this algorithm as Quantum Diffusion Control.

5 Annealed diffusion control for unitary dynamics

We present an annealing variant of QDC for optimal control of unitary dynamics. This approach leverages the extra freedom inherent in the Lindblad dissipation term $\mathcal{D}[D, C]$ to create annealing control protocols that bridge open and closed quantum system dynamics.

In this context, the dissipation superoperator $\mathcal{D}[D, C]$ is treated as a parametrized linear operator \mathcal{D}_p ($p = 1, \dots, n_{IS}$) in the importance sampling step p , which we assume compatible with the PI formalism. The operator \mathcal{D}_p is designed to interpolate the operator \mathcal{D}_p from a regime with high dissipation at the start of the training ($p = 1$) to one with low dissipation at the end of training ($p = n_{IS}$). This interpolation forms the basis of an annealing control protocol ansatz.

In this framework, QDC functions as a quantum control annealer. The initial phase of training corresponds to a high-temperature regime analogous to simulated annealing, where the search process is exploratory and exhibits high variance. As training progresses, the dissipation gradually diminishes, and in the final stage—the low-temperature phase—the system enters a cooling regime. At this stage, dissipation effects are negligible, and the simulated dynamics approach those of a purely unitary evolution.

Since the primary goal is achieving the optimal control of unitary dynamics, there is significant flexibility in designing an appropriate annealing protocol \mathcal{D}_p . This involves choosing a suitable set of Lindblad operators C and a noise matrix D , both of which can be parametrized in p . A straightforward example is to keep the dissipators C constant and set the noise matrix to be proportional to the identity matrix, $D = sI$, where $s > 0$ is a real parameter. A schedule s_p can then be constructed such that s_1 is relatively large, and decreases to $s_{n_{IS}} \ll 1$ at the end of the training. In Section 6.3 we demonstrate the utility of this approach to compute optimal controls for a multi-qubit spin system.

6 Numerical experiments

In this section we demonstrate through several examples the practicality and flexibility of our algorithm in solving different quantum control problems of interest. One could, in principle, build feedback control solutions using Eq. (12), as approximations of the underlying optimal feedback control $u^*(t, \psi_t)$, which takes into account the stochasticity of ψ_t . Given that is unrealistic to assume full observability of ψ_t at all times, and that a proper study including the measurement process is beyond the scope of this work, we restrict our analysis to open-loop control. For our experiments, we assume piece-wise constant controls over K time intervals. We parametrize the controls according to (12), and

⁴This can be easily seen. The dynamics in (20) is of the form

$$d\psi = f dt + g_a(u_a dt + dW_a)$$

with complex valued vector functions f and g_a . We write $d\psi, f, g_a$ in terms of their real and imaginary components $j = r, i$:

$$d\psi^j = f^j dt + g_a^j(u_a dt + dW_a)$$

which is already in path integral form.

write

$$u_a(t) = \sum_{k=1}^K u_{ak} \delta_{t \in I_k} \quad a = 1, \dots, n_c \quad (21)$$

with $I_k = [\tau_{k-1}, \tau_k]$, u_{ak} the k -th pulse corresponding to control u_a , and n_c the total number of controls. We use the Euler-Maruyama integration scheme for simulating the stochastic dynamics (20).

6.1 Control of a noisy qubit

Consider a single-qubit system evolving according to the Lindblad equation (39) with $H = u_x H_x + u_y H_y$, where $H_x = \sigma_x$ and $H_y = \sigma_y$. The dissipation part is given by the two non-Hermitian operators $C_1 = \sigma^+$ and $C_2 = \sigma^-$, where $\sigma^\pm = \frac{1}{2}(\sigma_x \pm i\sigma_y)$. This system is commonly used for modeling the emission and absorption of light quanta in a two-level system coupled to an electromagnetic field, e.g. a cavity resonator [33]. Assume a diagonal noise matrix $D_{ab} = D\delta_{ab}$. The Lindblad equation is

$$\dot{\rho} = -i[H, \rho] + D \left(\sigma^+ \rho \sigma^- + \sigma^- \rho \sigma^+ - \rho \right) \quad (22)$$

To propose an unraveling suitable for PI formulation, we transform the dissipators to a pair of anti-Hermitian operators using (3) with $\tilde{C}_1 = -iH_1$, $\tilde{C}_2 = -iH_2$ and

$$A = \begin{pmatrix} -i & -1 \\ -i & 1 \end{pmatrix} \quad (23)$$

and $\tilde{D}_{ab} = \frac{1}{2}D\delta_{ab}$. The unraveling (20) becomes:

$$d\psi = -\tilde{D}\psi dt - i\sigma_a \psi (u_a dt + dW_a) \quad (24)$$

where $a = x, y$. As stated in Sec. 2, this unraveling preserves the norm of ψ . This implies that the stochastic trajectories generated by (24) lie on the Bloch sphere.

We use as cost Eq. (19), subject to $R\tilde{D} = \lambda$. We consider the state preparation problem from an initial state $\psi_0 = |X\rangle := \frac{1}{\sqrt{2}}(|0\rangle + |1\rangle)$ to a target state $\phi = |Y\rangle := \frac{1}{\sqrt{2}}(|0\rangle + i|1\rangle)$. Although the transformation $X \rightarrow Y$ can be realized by a simple σ_z rotation, this task is non-trivial, since σ_z is not one of the control primitives in H . Instead, σ_x, σ_y must coordinate so as to realize the desired rotation. As a result, the optimal trajectories do not lie on the equator.

In Fig. 1 (A) we show the adaptive importance sampling. We plot the average fidelity over trajectories F_{avg} , the worse case fidelity over trajectories F_{min} and the average control cost C in (19) versus IS steps. In addition, we plot the effective sample size ESS in (11), which is a sensitive measure of the quality of the optimal control solution. The ESS indicates how close the control solution is to the optimal (feedback) control, for which $ESS = 1$. We observe that while the fidelity and control cost converge fast to constant values, the ESS still increases indicating that the quality of the control solution is still improving (shaded region). We observe that the control solution becomes smoother in these later IS iterations. The asymptotic average fidelity for $K = 128$ is $F^* = 0.9759 \pm 0.0006$. Since the optimal control solution is a compromise between the final fidelity and the fluence $U := \int_0^T u^T(t)u(t)$, higher fidelity solutions can be obtained by lowering R in Eq. (19). Indeed, by reducing $R = 1$ to $R = 0.1$ the average asymptotic fidelity increases to $F^* = 0.9963 \pm 0.0002$. Fig. 1 (B) shows one of the two optimal control solutions $u_{x,y}(t)$ after convergence of the IS training. The other solution is obtained by taking $u_{x,y}(t) \rightarrow -u_{x,y}(t)$. In Fig. 1 (C) we show how the quality of the optimal control solution in terms of asymptotic ESS depends on the number of pulses K . The ESS increases monotonically until reaching an asymptote at around $ESS \sim 0.21$, showing the sub-optimality of the open-loop control compared to the optimal feedback solution (for which $ESS = 1$). Fig. 1 (D) shows quantum trajectories on the Bloch sphere under optimal control.

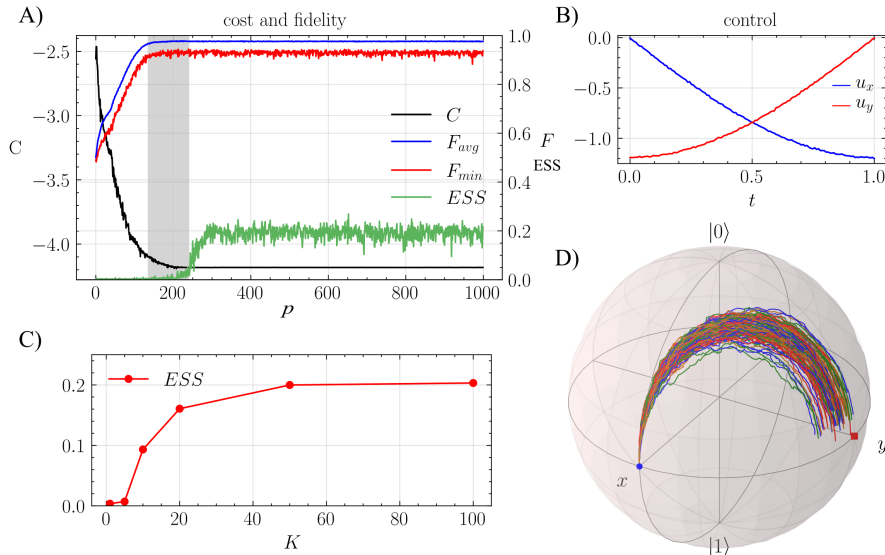


Figure 1: Control of a noise qubit from $X \rightarrow Y$. (A) Average fidelity F_{avg} , minimal fidelity F_{min} , effective sample size ESS and cost C in 19 versus importance sampling iterations p . The converged average fidelity is $F^* = 0.9759 \pm 0.0006$. (B) Optimal control solution $u_{x,y}(t)$ after convergence of the algorithm. The optimal solution is two-fold degenerate. The two solutions are related by a global sign $u_{x,y} \rightarrow -u_{x,y}$. (C) Dependence of the quality of the optimal control, measured by the ESS, on the number of pulses K . (D) Optimally controlled trajectories on the Bloch sphere. Parameters: final time $T = 1$, noise coupling $D = 0.005$, control weight $R = 1$, fidelity weight $Q = 10$, number of pulses $K = 128$, number of trajectories $N_{tra,j} = 400$ per IS step, maximum number of IS steps $n_{IS} = 1000$ and time discretization $dt = T/N_T$ with $N_T = 128$. IS smoothing window $w = 40$ (see Section 3.1).

Benchmark with Open GRAPE.— As benchmark, we compare the performances of QDC and (first order) Open GRAPE algorithm [27], which computes coherent controls for the Lindblad equation. See the Supplementary Material for details on the algorithm and implementation. We solve the state preparation problem $X \rightarrow Y$ for the single qubit using $K = 128$ pulses. The control problem is defined by the Lindblad equation (22) and the cost function (18).

We run QDC and Open GRAPE algorithms 505 times using random control initializations drawn from both normal and uniform distributions. Regarding the stopping condition for Open GRAPE, the optimization stops when the cost cannot be further optimized by decreasing the learning rate; see App. 3 for details. In the case of QDC algorithm, the optimization runs for a maximum of 800 IS steps, ensuring that the algorithm reaches convergence in every run.

In Fig. 2 we show the distribution of control costs (along the fidelities and fluences) for Open GRAPE (main panels) and QDC (insets). We mark the average cost, fidelity and fluence of QDC solutions by a yellow dot in each graph. The QDC solutions have lower cost than the Open GRAPE solutions. The width of the dashed vertical lines locating each mean is much larger than the standard deviation of each QDC distribution, showing that the variance of QDC solutions is very narrow compared to that of Open GRAPE ones. Open GRAPE converges to many different solutions with different costs depending on the initial condition. Instead, QDC converges consistently to one of two solutions with same cost, fidelity, fluence and effective sample size, which are related by a global sign (Fig. 1 (B)). The difference between individual solutions has RMS error less than $\mathcal{O}(10^{-4})$. By direct inspection we can also verify that these profiles correspond to two different underlying smooth solutions. We conclude that the different QDC solutions, rather than representing local minima, correspond to the same underlying solution up to small statistical fluctuations due to the stochastic nature of the algorithm.

We further compare these two algorithms' solutions by performing a t-SNE embedding [68] over Open GRAPE solutions together with QDC solutions. In Fig. 3 (A) we plot some of the most regular

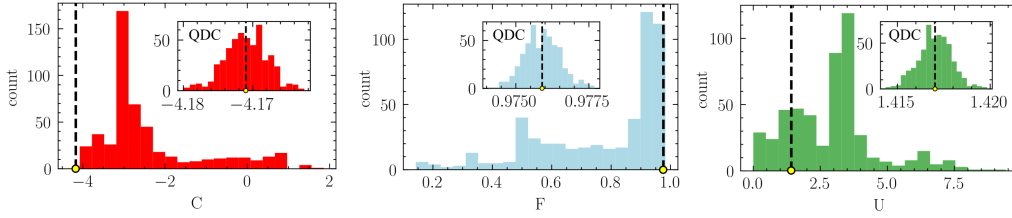


Figure 2: Histograms of optimal control costs obtained with Open GRAPE (main panel) and QDC (inset) on 505 runs. For Open GRAPE, the average cost, fidelity and fluence (and standard deviations) are $\langle C \rangle = -4 \pm 1$, $\langle F \rangle = 0.8 \pm 0.2$ and $\langle U \rangle = 3 \pm 2$, respectively. The minimum cost achieved is $C_{min} = -4.07$. For QDC, the corresponding average values (yellow dot) are $\langle C \rangle = -4.171 \pm 0.003$, $\langle F \rangle = 0.9759 \pm 0.0006$ and $\langle U \rangle = 1.4170 \pm 0.0009$. In the main panels, the dashed vertical lines at the QDC average are wider than the actual standard deviations of the QDC distributions. This illustrates the large difference in variance between the two methods. All QDC runs converge to solutions with the same cost, fidelity, fluence and effective sample size up to small statistical fluctuations due to the stochastic nature of QDC algorithm. Parameter setting: $D = 0.005$, $T = 1$, $R = 1$, $Q = 10$, $K = 128$, $w = 20$.

Open GRAPE control solutions. In Fig. 3 (B) we show the t-SNE embeddings for $[u_x, u_y]$, considered as a vector of length $2K$. Each dot represent a different Open GRAPE solution and we represent the (average) QDC solutions with yellow dots. We further perform a K-means decomposition to cluster the different solutions into 3 clusters (colored with red, blue and black). The different Open GRAPE solutions tend to cluster around each ground truth QDC solution. In Fig. 3 (C) we plot the average profiles of the Open GRAPE solutions of cluster 1 (red) and cluster 2 (blue) together with the average QDC profiles. The qualitative resemblance between the averages and the QDC solution indicates that the Open GRAPE local minima tend to cluster around the ground truth solutions represented by QDC solutions. The cluster colored with black consists of local minima control solution of Open GRAPE with high control cost C .

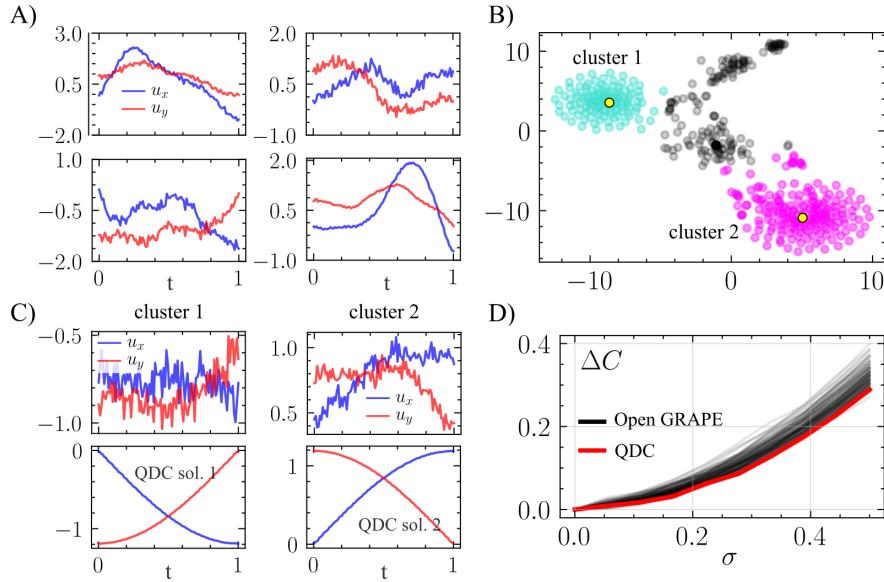


Figure 3: (A) Examples of Open GRAPE solutions with diverse levels of regularity for different seeds. (B) 2-D t-SNE dimension reduction representation followed by a K-means decomposition of Open GRAPE solutions (red, blue and black dots) and the two average QDC solutions (yellow dots). The cluster of black dots correspond to local minima of relatively high cost C . (C) Average Open GRAPE solutions for cluster 1 (red) and cluster 2 (blue). In the bottom panels, the QDC solutions corresponding to each cluster. (D) Robustness $\Delta C = C(u + \xi) - C(u)$ versus σ with u the high-fidelity high-ESS QDC solution (red) and the high-fidelity low-ESS Open Grape solution (black).

During the IS iterations of the QDC algorithm, the optimization keeps improving in terms of ESS, even when maximum fidelities are reached; see shaded area in Fig. 1. Instead, Open GRAPE solutions, while having similar fidelities as the QDC solution, have low $ESS = \mathcal{O}(10^{-3})$. We expect that the high fidelity, high-ESS QDC solutions are more robust to random perturbations than the high fidelity, low-ESS Open GRAPE solutions. We test this by perturbing the optimal control solution $u(t) \rightarrow u(t) + \xi(t)$ with $\xi(t)$ with Gaussian perturbations with mean zero and standard deviation σ and compute the maximal cost difference $\Delta C = C(u + \xi) - C(u)$ for 20 different noise realizations. We compare high-fidelity low-ESS Open GRAPE solutions, defined by having a cost $C < -3.8$ with the high fidelity high ESS QDC solution in Fig. 3 (D) for different σ . For completeness, we also include in the experiment the high-fidelity low-ESS QDC solutions corresponding to the shaded area of Fig. 1 (A). It can be observed that the QDC solution (in red) is more robust to random perturbations than low-ESS Open GRAPE solutions (in black). Therefore, we conclude that the ESS is a useful additional criterion to assess the quality in terms of the robustness of the (open loop) control solution.

6.2 Leveraging open-system solutions for unitary dynamics

The dynamics of the average state $\langle \psi \rangle$ follows the equation

$$d \langle \psi \rangle = -i(H_e + H_u) \langle \psi \rangle dt \quad (25)$$

where $H_e = H_0 - \frac{i}{2} D_{ab} H_a H_b$ and $H_u = u_a H_a$. Provided that the norm of the correction term $D_{ab} H_a H_b$ is sufficiently small, we expect the solution of the open control problem to work well for the unitary case $D = 0$. Conversely, we expect this correspondence to degrade as D increases. The question is then to which extent we can leverage the solution of the open control problem to achieve high fidelities in the unitary case.

We explore this question for the noisy qubit. We compare the fidelity scores for the open and closed system for different noise values D . We consider the $X \rightarrow Y$ state preparation problem. For each D , we compute a control u that achieves maximal average fidelity F_{open} for the open case, and use it to steer the unitary dynamics in the time interval $[0, T]$. Then, we compare F_{open} with the fidelity achieved at time T in the unitary case, which we denote F_{closed} . See Fig. 4 (A).

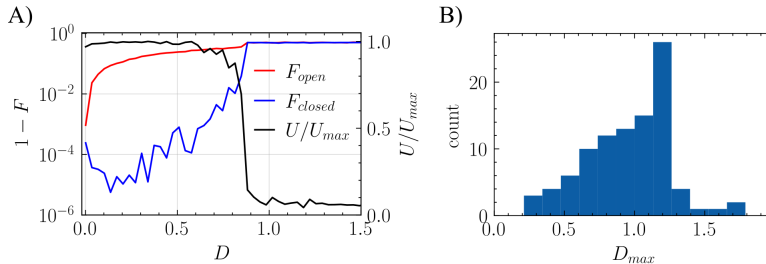


Figure 4: (A) Single qubit, $X \rightarrow Y$. In the left y-axis, fidelities F_{open} and F_{closed} vs D ; in the right y-axis, normalized fluence U/U_{max} , vs D , with $U_{max} = 1.86$. Parameters: $T = 1$, $K = 50$, $R = 0.5$, $N_T = 100$, $N_{traj} = 2000$ and Q iterates over 5, 50 and 100, and stopping when the fidelity threshold condition $F_{avg} > 0.98$ is met. (B) $X \rightarrow Haar$. Distribution of D_{max} for 100 random Haar target states. Average $\langle D_{max} \rangle = 1 \pm 0.3$.

Surprisingly, the unitary dynamics reaches high fidelities for a wide range of noise values, even when F_{open} deteriorates fast as D increases. Moreover, the closed-system fidelity F_{closed} reaches a minimum at a later value of D . This is not surprising, as the sampling becomes harder and needs more trajectories at close-to-zero values of D to maintain estimation efficiency. This high-temperature effect is closely related to the annealing QDC technique that we explore in Sec. 6.3.

Both, the open and the unitary dynamics, show a sharp transition in the fidelity at a certain noise value D_c . This point also corresponds with a fast decrease in the fluence. We remark that this phase

transition is particular to the $X \rightarrow Y$ problem, and is not necessarily present for other control paths $A \rightarrow B$, for arbitrary states A and B .

Nonetheless, the open system solution u demonstrates robustness across a range of D values for other control paths as well. We quantify this by repeating the previous experiment for random Haar target states, and fixed initial state $\psi_0 = |0\rangle$ ($X \rightarrow \text{Haar}$). For each problem, we record the maximum noise value D_{max} for which the fidelity F_{closed} is above 0.98. In Fig. 4 (B), we show the distribution of D_{max} for 100 random Haar states. These results indicate that the QDC algorithm can also be used for computing the optimal controls for unitary dynamics.

6.3 GHZ states on open NMR systems

In this section, we test the capability of our algorithm in handling systems with multiple qubits. We demonstrate that our QDC algorithm can successfully prepare states for realistic systems such as NMR molecules. NMR quantum computing has gained significant popularity in recent years as a testbed technology for experimental and theoretical research due to the long coherence times attained compared to the dynamical scales of the system [69]. NMR systems are defined by a total Hamiltonian $H = H_0 + H_c$, where H_0 is the drift and H_c is the control part. The drift and control Hamiltonians are further defined as

$$H_0 = H_Z + H_I \quad H_c = \sum_{i=1}^n u_{ix}\sigma_i^x + u_{iy}\sigma_i^y \quad (26)$$

where $H_Z = \sum_{i=1}^n \pi\nu_i\sigma_i^z$ and $H_I = \sum_{i<j}^n \frac{\pi}{2}J_{ij}\sigma_i^z\sigma_j^z$. The constants ν_i denote self-energies, commonly called chemical shifts, and J_{ij} are the coupling strengths between the different spins in the system. Pulse-based control is a common approach to control NMR systems. It consists in the sequential application of external radio-frequency pulses across the x - y plane. These pulses are represented by time-dependent fields u_{ia} acting on each qubit i along x and y directions. Configurations like (50) have been proven fully controllable in the sense of state preparation [70], initially rendering NMR systems strong candidates for universal quantum simulators [71].

Due to the typical large difference in magnitude between H_Z and H_I , it is common practice to work in a rotating frame where the dynamics induced by H_Z is absent. Operationally, the rotating frame has the effect of setting $H_Z = 0$ in the drift Hamiltonian H_0 . The optimized pulses in the rotating frame can then be easily transformed back to the laboratory frame. We write the details about the rotation frame approach and the proof of control equivalence in the Supplementary Material.

We write the Lindblad equation for the NMR system as

$$\dot{\rho} = -i[H, \rho] + D \sum_{i=1}^n \left(\sigma_i^- \rho \sigma_i^+ + \sigma_i^+ \rho \sigma_i^- - \rho \right) \quad (27)$$

where $H = H_I + H_c$ and dissipation σ_i^\pm of equal strength D acting on individual spins. The control cost is defined as

$$C = -\frac{Q}{2} \left\langle \mathcal{F}(\psi_T) + \frac{R}{2} \int_0^T \left(\sum_{i=1}^n \sum_{a=x,y} u_{ia}^2(t) \right) dt \right\rangle \quad (28)$$

We assume for simplicity, both, $R \rightarrow R/n_c I$ and $D \rightarrow DI$, proportional to the identity matrix I , with constants R, D , respectively, and n_c the number of control components; $n_c = 2n$ for NMR. As in the case of one qubit, we use the transformation (23) to convert the non-Hermitian operators $C_{ia} = \sigma_i^a$, $a = \pm$ in Eq. (27) into anti-Hermitian operators

$$\tilde{C}_{ib} = C_{ia} A_{ab} \quad \text{for all } i \quad (29)$$

This leads to the following expression for the transformed operators

$$\tilde{C}_{ib} = -i\sigma_i^b \quad \text{for all } i \text{ and } b = x, y. \quad (30)$$

and $\tilde{D} = \frac{1}{2}D$. This transformation leaves the Lindblad equation (27) invariant. The corresponding unraveling is

$$d\psi = -iH_I\psi dt - i\left(\sum_{i=1}^n \sum_{a=x,y} (u_{ia}dt + d\tilde{W}_{ia})\sigma_i^a\right)\psi - n\tilde{D}\psi dt \quad (31)$$

with $\langle d\tilde{W}_{ia}d\tilde{W}_{jb} \rangle = \delta_{ij}\delta_{ab}\tilde{D}dt$ for $i, j = 1, \dots, n$ and $a, b = x, y$. Equations (28) and (31) define a path integral control problem with $\lambda = \tilde{D}R$. The initial state is $\psi_0 = |0\rangle^{\otimes n} = Z^{\otimes n}$. We choose the target state ϕ to be a Greenberger–Horne–Zeilinger (GHZ) state, which is defined as $|GHZ_n\rangle := \frac{1}{\sqrt{2}}(|0\rangle^{\otimes n} + |1\rangle^{\otimes n})$ for n -qubit systems and it represents a maximally entangled state in the global entanglement (or Meyer-Wallach) measure for multipartite systems [72]. In the rotating frame, the target state takes the form $\phi = \frac{1}{\sqrt{2}}(e^{i2\pi\omega T}|0\rangle^{\otimes n} + e^{-i2\pi\omega T}|1\rangle^{\otimes n})$ with $\omega = \frac{1}{2}\sum_j \nu_j$.

For comparison, we consider the 4-qubit NMR example of [73]. We take the shifts ν_i and couplings J_{ij} from Table I therein. In [73] authors use an iterative version of GRAPE, called i-GRAPE, to optimize the pulses. GRAPE-like methods need, in general, a high number of pulses to validate and find good solutions. As a result, those solutions tend to be very irregular. In addition, the variation is high between solutions for different runs, and the reported solutions for GRAPE and i-GRAPE are very different between each other. In QDC, on the other hand, this is not a constraint and the number of pulses can be arbitrary. Whether the solutions achieve high fidelities or not depends on other factors, such as controllability or the cost parameters. This difference arises from the distinct approach in dealing with time correlations in QDC; we return to this point in Sec. 7.

We prepare a GHZ state for the 4-qubit NMR molecule coupled to an environment. The dynamics corresponds to the Lindblad equation (27). We set the noise coupling $D = 1/T_1$, with T_1 the minimum relaxation time [73]. To compare with the unitary analog in [73], we choose the same final time, $T = 8.8$. In Fig. 5 (A) we show in red the infidelity $1 - F_{avg}$ reached after convergence for different values of K . In the unitary case, authors in [73] report solutions with infidelity 2×10^{-3} with $K = 1760$

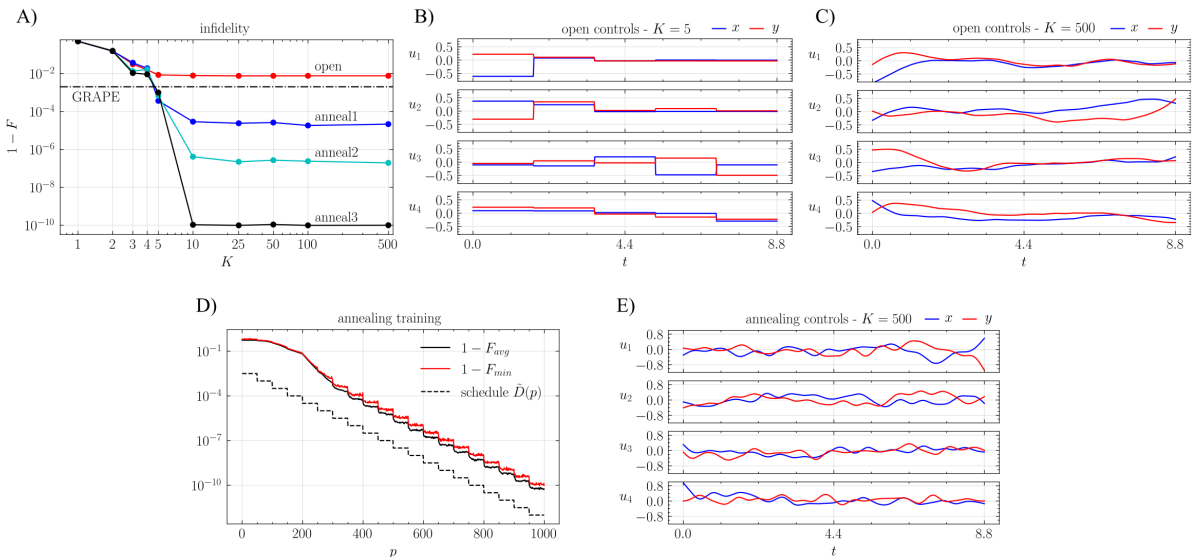


Figure 5: 4-NMR control. (A) Infidelity $1 - F$ vs K . Curve open corresponds to the open system case, with fixed noise coupling $D = 1/T_1$. Curves anneal1, anneal2 and anneal3 correspond are the infidelities using annealing control. The rest of parameters are: $N_T = 500$, $n_{IS} = 1000$. We show the control solutions for the open system case for $K = 5$ pulses (B) and $K = 500$ pulses (C). In panel (D) we show an example of annealing training for $K = 500$ pulses and logarithmic end cost. We plot the average and the worst case infidelities as function of the IS step, and in panel (E) we plot the corresponding final solutions. These solutions achieve a infidelity of 6×10^{-11} .

GRAPE pulses. In the noisy case, we achieve infidelities less than 1×10^{-2} for $K = 5$ pulses (B). These

same control solutions achieve infidelity less than 8×10^{-4} in the noiseless case. In Fig. 5 (C) we show a solution corresponding to $K = 500$ pulses. In this case, the controls are iteratively smoothed during the importance sampling using cubic splines. For large K , this enforces the search to look for smooth solutions without sacrificing accuracy.

In Section 6.2 we explored the question of whether we can leverage the solutions computed in the open system case as proxy solutions for the corresponding unitary dynamics. Here we apply the annealing diffusion control described in Sec. 5 to directly compute optimal controls for the unitary case. We parametrize \tilde{D} in (31) in the importance sampling step p , interpolating between two noise values: a high initial noise \tilde{D}_0 , and a much lower noise $\tilde{D}_f \ll 1$. The particular form of the annealing schedule $\tilde{D}(p)$ is treated as an ansatz. We apply this technique to the 4-NMR case. Empirically, we found that good schedules allow the algorithm to sample the control landscape more effectively in early stages of the optimization to converge to good solutions. We choose a piece-wise constant schedule composed of d_i ($i = 1, \dots, N_{steps}$) values distributed equidistantly in the IS interval. In the i -th IS interval, the noise value $d_i := D_0 \left(\frac{D_f}{D_0}\right)^{(i-1)/(N_{steps}-1)}$. Here we set $N_{steps} = 20$, $D_0 = 3 \times 10^{-3}$ and $D_f = 1 \times 10^{-12}$; see dashed line in Fig. 5 (D). In panel (A) we plot the infidelity $1 - F$ vs K , for different configurations in the control parameters. Curves **anneal1** and **anneal2** correspond to $Q = 400$ and $Q = 4000$, respectively, keeping $R = 1$ fixed. The annealing training is performed using an averaging window $w = 10$ in the first 200 IS steps, then setting $w = 1$ for the rest of the training. The result represents an improvement in infidelity of 2 and 4 orders of magnitude, respectively, with respect to GRAPE [73]. Furthermore, by changing to a logarithmic end cost $\Phi(\psi_T) = \frac{Q}{2} \log(1 - \mathcal{F}(\psi_T))$, we get an improvement of 7 orders of magnitude with respect to GRAPE; see **anneal3** (A). For this last case, we show in panel (D) the infidelity training curves for $K = 500$, and the corresponding smoothed annealed solutions in panel (E). As for the open case, the smoothing was performed during training, using cubic splines. This experiment demonstrates that QDC can be effectively used as an annealer to find high quality controls for unitary dynamics.

7 Discussion

The main features of our method can be summarized as follows: 1) it is *state-centered*: the quantum trajectories are obtained by propagating state vectors of size N , opposed to most common density-based approaches, which require propagating density matrices of size N^2 ; in this way, our algorithm inherently comprises a quadratic advantage in runtime over density-based methods, such as the PMP method or the adjoint method [29]. 2) it is *embarrassingly parallel*: The core of QDC computation is to learn a model on the basis of self-generated data (sample trajectories) and this procedure is iterated using improved controls until convergence. The importance sampling updates Eqs. (14) and (16) can be very efficiently parallelized by noting that the gradient consists of a sum over the data and that the computation of this sum can be distributed over m machines so that the updated parameters $\theta_{p+1} = \theta_p + \frac{1}{m} \sum_{i=1}^m d\theta_p^{(i)}$ with $d\theta_p^{(i)}$ the gradient update computed on machine i . No large volumes of simulated raw data need to be transferred between machines, only the parameter updates. See Fig. 6 (left). This results in close-to-linear speedup.

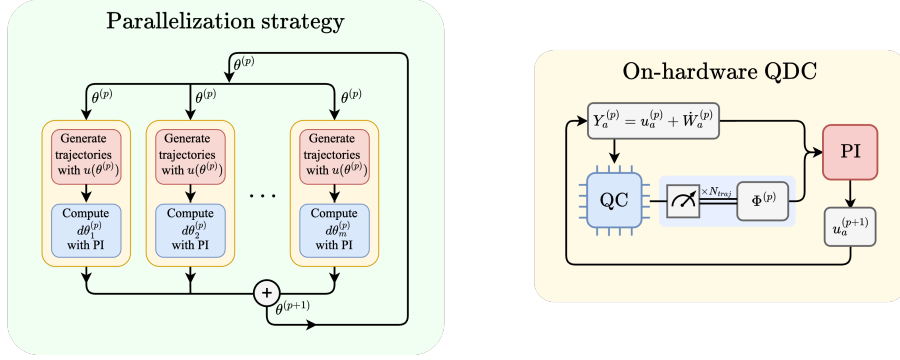


Figure 6: **(Left)** During each iteration, samples are generated using control functions $u(\theta^{(p)})$. These samples are used to compute new parameters $\theta^{(p+1)}$. These two steps can be distributed on many machines with minimal communication overhead, since no large volumes of simulated raw data need to be transferred between machines, only the parameter updates. **(Right)** At each IS step p , simulate in the quantum computer (QC) N_{traj} unitary trajectories with input control signal $Y_a^{(p)} = u_a^{(p)} + \dot{W}_a^{(p)}$, where $u_a^{(p)}$ is the control trajectory and $\dot{W}_a^{(p)}$ are the N_{traj} self-generated noise trajectories. At time T , measure the state and produce N_{traj} measurements $\Phi^{(p)} = \psi_T^{(p)\dagger} H_{\text{target}} \psi_T^{(p)}$. Input the current control, the noise trajectories and the measurements into the IS formula (17) and update the control to $u_a^{(p+1)}$. Repeat.

3) An important point concerns the nature of the control computation in QDC. For any control problem, the primary computational challenge lies in quantifying the influence of early control actions on the system's state and cost at later times. For instance, GRAPE and PMP use some form of backward evolution of the co-state to estimate this dependence. QDC, instead, uses an entirely different mechanism, by generating forward-sampled stochastic-particle trajectories that are weighted with their exponentiated control cost. These global statistics are then used to update the parameters in each time bin independently. This is a prominent feature of our QDC algorithm and stands out from other methods where a direct access to the objective gradients is needed. Our experiments suggest that this is may represent a more effective way to compute the optimal control, when the control problem is of the PI form.

7.1 A proposal for on-hardware QDC

The QDC algorithm includes a subroutine for simulating quantum trajectories of the stochastic dynamics described by (20), and this scales exponentially on classical hardware. Other QOC approaches suffer from the same curse, for which replacing classical simulation by quantum hardware implementations seems not only favorable for better scaling but necessary. Here, we propose a way to run the QDC framework on quantum hardware. The following can be seen as a realization of a quantum-classical optimization protocol [74], where the optimization part is achieved by PI control. The crucial observation is that the stochastic dynamics dictated by (20) can be interpreted as a random unitary dynamics [67]. This dynamics is defined by a Hamiltonian $H = H_0 + H_c$, where $H_c = Y_a H_a$ is determined by a random control signal $Y_a = u_a + \dot{W}_a$, composed by a deterministic part u_a , and a stochastic part \dot{W}_a —the time derivative of the Wiener process is formal, and should be interpreted in the discrete sense. Given a suitable time discretization dt , we can replace the subroutine with the classical simulations of the open dynamics (20) by simulations on the actual quantum hardware.

In Fig. 6 (right), we show a flow diagram illustrating the on-hardware QDC algorithm's operation for a general end cost $\Phi(\psi_T) = \psi_T^\dagger H_{\text{target}} \psi_T$, with H_{target} an arbitrary Hermitian matrix. The algorithm's fundamental operation involves iterative state preparations and measurements to optimize the quantum dynamics. The computational complexity, in terms of required re-preparations and measurements, follows a scaling $\propto \frac{\alpha}{\varepsilon_q^2 \varepsilon_c^2}$ [74]. Here, $\alpha = \mathcal{O}(\text{poly}(n))$ with n the system's size, and ε_q and ε_c denote the precision requirements for quantum and classical expectation value estimations, respectively, in the

on-hardware QDC loop. This naive scaling can be substantially improved through better estimation techniques and the parallelization strategies discussed earlier.

We remark that the on-hardware implementation of QDC can be realized either, at the circuit level, or pulse level. In the first, the optimization targets parametrized quantum gates encoding the quantum dynamics. The control parameters are the gate parameters within the quantum circuit. Variational quantum algorithms (VQAs) operate in this level. The pulse level operates below the circuit level, and involves direct optimization of the Hamiltonian dynamics through successive applications of electromagnetic pulses, analogous to the NMR control described in Sec. 6.3. Here, the control parameters are the actual physical fields driving the quantum system. Methods for commuting between these two levels have been extensively studied [75], establishing the circuit level as a well-defined abstraction layer above the physical pulse level [74].

Pulse-based control may offer several potential advantages over circuit-based control. For instance, on four transmon qubits, a reduction in state preparation time of roughly three orders of magnitude compared to gate based strategies was demonstrated [76]. More recently, authors [77] have recently applied pulse-based optimal control for ground state preparation, demonstrating that pulse-based control required less time than an equivalent digital circuit. These approaches restrict to closed quantum systems and open loop control. The QDC method provides a realistic and computationally tractable approach to extend this work in the direction of open quantum systems and feedback control. A comprehensive analysis comparing QDC performance with state-of-the-art variational quantum algorithms [76, 77], including detailed benchmarking results, will be addressed in future work.

8 Conclusion and Outlook

In this work we propose Quantum Diffusion Control (QDC), a novel approach for optimal control of open quantum systems. We bring together tools from path integral control and quantum trajectories to frame a broad class of quantum control problems in the language of stochastic optimal control theory. Stochastic optimal control problems usually demand the integration of a Hamilton-Jacobi-Bellman equation, which is prohibitive for large systems. QDC bypasses this requirement giving the optimal solution explicitly as a path integral. Optimal controls are then computed by sampling stochastic trajectories in the Hilbert space. The path integral formulation of the control problem unlocks the possibility of integrating Monte Carlo and Machine Learning techniques directly into the estimation process. Here, we use adaptive importance sampling, a scheme where the controls are incrementally improved and the optimal control solutions are seen as fixed points of this process. For linear parametrizations, either open-loop or feedback, the importance sampling updates are computed as stochastic averages, as given by Eqs. (14) and (16). We remark that, for linear parametrizations, such as in pulse-based control, our method offer closed-form expressions for the optimal controls. The efficiency of the control computation is dictated, in this case, by the quality of the estimation. For non-linear parametrizations –e.g., when the control functions $u(\theta)$ are represented by deep neural networks –a more general adaptive importance sampling algorithm is given by the Path integral Cross-Entropy (PICE) method [78], involving the gradients $\partial u/\partial \theta$. As in any neural network training, these gradients can be computed using automatic differentiation [79].

The QDC algorithm, including the importance sampling method and their generalization to PICE, automatically compute feedback control solutions, although under the unrealistic assumption of full observability of the quantum state for all times. Since the state is partially observable only through measurement, the control problem becomes what is known as a *partial observable control problem* [80]. Extending QDC to (practical) feedback control requires the incorporation in the loop of the measurement process. A compromise between information gain and minimal disruption of the quantum state is given by the so-called *weak or continuous measurement* [81–83]. The extension of our approach to incorporate partial observation and continuous measurements is currently under development and will be presented in future work.

We hope this work contributes and foster the cross-fertilization between path integral control tech-

niques and quantum control methods, towards scalable and efficient control of open quantum systems.

References

- [1] Daniel A Lidar and Todd A Brun. *Quantum error correction*. Cambridge university press, 2013.
- [2] Iulia M Georgescu, Sahel Ashhab, and Franco Nori. “Quantum simulation”. In: *Reviews of Modern Physics* 86.1 (2014), pp. 153–185.
- [3] Vittorio Giovannetti, Seth Lloyd, and Lorenzo Maccone. “Advances in quantum metrology”. In: *Nature photonics* 5.4 (2011), pp. 222–229.
- [4] Christian L Degen, Friedemann Reinhard, and Paola Cappellaro. “Quantum sensing”. In: *Reviews of modern physics* 89.3 (2017), p. 035002.
- [5] Juan M Arrazola et al. “Quantum circuits with many photons on a programmable nanophotonic chip”. In: *Nature* 591.7848 (2021), pp. 54–60.
- [6] SLN Hermans et al. “Qubit teleportation between non-neighbouring nodes in a quantum network”. In: *Nature* 605.7911 (2022), pp. 663–668.
- [7] Pascal Baßler et al. “Synthesis of and compilation with time-optimal multi-qubit gates”. In: *Quantum* 7 (2023), p. 984.
- [8] Pavel Bushev et al. “Feedback Cooling of a Single Trapped Ion”. en. In: *Physical Review Letters* 96.4 (2006), p. 043003. ISSN: 0031-9007, 1079-7114. DOI: [10.1103/PhysRevLett.96.043003](https://doi.org/10.1103/PhysRevLett.96.043003). URL: <https://link.aps.org/doi/10.1103/PhysRevLett.96.043003> (visited on 08/13/2024).
- [9] Massimiliano Rossi et al. “Measurement-based quantum control of mechanical motion”. en. In: *Nature* 563.7729 (2018). Publisher: Nature Publishing Group, pp. 53–58. ISSN: 1476-4687. DOI: [10.1038/s41586-018-0643-8](https://doi.org/10.1038/s41586-018-0643-8). URL: <https://www.nature.com/articles/s41586-018-0643-8> (visited on 08/13/2024).
- [10] Charles S Adams, Jonathan D Pritchard, and James P Shaffer. “Rydberg atom quantum technologies”. In: *Journal of Physics B: Atomic, Molecular and Optical Physics* 53.1 (2019), p. 012002.
- [11] Loïc Henriët et al. “Quantum computing with neutral atoms”. In: *Quantum* 4 (2020), p. 327.
- [12] Lorenzo Magrini et al. “Real-time optimal quantum control of mechanical motion at room temperature”. en. In: *Nature* 595.7867 (2021). Publisher: Nature Publishing Group, pp. 373–377. ISSN: 1476-4687. DOI: [10.1038/s41586-021-03602-3](https://doi.org/10.1038/s41586-021-03602-3). URL: <https://www.nature.com/articles/s41586-021-03602-3> (visited on 08/13/2024).
- [13] Steffen J. Glaser et al. “Training Schrödinger’s Cat: Quantum Optimal Control: Strategic Report on Current Status, Visions and Goals for Research in Europe”. In: *The European Physical Journal D* 69.12 (Dec. 2015), p. 279. ISSN: 1434-6060, 1434-6079. DOI: [10.1140/epjd/e2015-60464-1](https://doi.org/10.1140/epjd/e2015-60464-1). URL: <http://link.springer.com/10.1140/epjd/e2015-60464-1> (visited on 05/23/2024).
- [14] Christiane P. Koch et al. “Quantum Optimal Control in Quantum Technologies. Strategic Report on Current Status, Visions and Goals for Research in Europe”. In: *EPJ Quantum Technology* 9.1 (Dec. 2022), p. 19. ISSN: 2662-4400, 2196-0763. DOI: [10.1140/epjqt/s40507-022-00138-x](https://doi.org/10.1140/epjqt/s40507-022-00138-x). URL: <https://epjquantumtechnology.springeropen.com/articles/10.1140/epjqt/s40507-022-00138-x> (visited on 05/23/2024).
- [15] Shuang Cong. *Control of quantum systems: theory and methods*. John Wiley & Sons, 2014.
- [16] Domenico d’Alessandro. *Introduction to quantum control and dynamics*. Chapman and hall/CRC, 2021.
- [17] TS Mahesh, Priya Batra, and M Harshanth Ram. “Quantum optimal control: Practical aspects and diverse methods”. In: *Journal of the Indian Institute of Science* 103.2 (2023), pp. 591–607.

- [18] Navin Khaneja et al. “Optimal control of coupled spin dynamics: design of NMR pulse sequences by gradient ascent algorithms”. In: *Journal of magnetic resonance* 172.2 (2005), pp. 296–305.
- [19] Yuquan Chen et al. “Accelerating quantum optimal control through iterative gradient-ascent pulse engineering”. In: *Physical Review A* 108.5 (2023). Publisher: American Physical Society, p. 052603. DOI: [10.1103/PhysRevA.108.052603](https://doi.org/10.1103/PhysRevA.108.052603). URL: <https://link.aps.org/doi/10.1103/PhysRevA.108.052603> (visited on 07/23/2024).
- [20] Tommaso Caneva, Tommaso Calarco, and Simone Montangero. “Chopped random-basis quantum optimization”. In: *Physical Review A* 84.2 (2011), p. 022326.
- [21] Vadim F Krotov. “Global methods in optimal control theory”. In: *Advances in nonlinear dynamics and control: a report from Russia*. Springer, 1996, pp. 74–121.
- [22] DJ Tannor et al. “Time-dependent quantum molecular dynamics”. In: *Nato ASI Series B* 299 (1992), p. 347.
- [23] Daniel M Reich, Mamadou Ndong, and Christiane P Koch. “Monotonically convergent optimization in quantum control using Krotov’s method”. In: *The Journal of chemical physics* 136.10 (2012).
- [24] Mohamed Abdelhafez, David I. Schuster, and Jens Koch. “Gradient-Based Optimal Control of Open Quantum Systems Using Quantum Trajectories and Automatic Differentiation”. In: *Physical Review A* 99.5 (2019), pp. 1–20. ISSN: 24699934. DOI: [10.1103/PhysRevA.99.052327](https://doi.org/10.1103/PhysRevA.99.052327). arXiv: [1901.05541](https://arxiv.org/abs/1901.05541).
- [25] U. Boscain, M. Sigalotti, and D. Sugny. “Introduction to the Pontryagin Maximum Principle for Quantum Optimal Control”. In: *PRX Quantum* 2.3 (Sept. 14, 2021), p. 030203. ISSN: 2691-3399. DOI: [10.1103/PRXQuantum.2.030203](https://doi.org/10.1103/PRXQuantum.2.030203). arXiv: [2010.09368](https://arxiv.org/abs/2010.09368) [quant-ph]. URL: <http://arxiv.org/abs/2010.09368> (visited on 05/23/2024).
- [26] Christiane P. Koch. “Controlling Open Quantum Systems: Tools, Achievements, and Limitations”. In: *Journal of Physics Condensed Matter* 28.21 (2016), pp. 1–14. ISSN: 1361648X. DOI: [10.1088/0953-8984/28/21/213001](https://doi.org/10.1088/0953-8984/28/21/213001). arXiv: [1603.04417](https://arxiv.org/abs/1603.04417).
- [27] Samuel Boutin et al. “Resonator reset in circuit QED by optimal control for large open quantum systems”. In: *Physical Review A* 96.4 (2017), p. 042315.
- [28] Michael H Goerz and Kurt Jacobs. “Efficient optimization of state preparation in quantum networks using quantum trajectories”. In: *Quantum Science and Technology* 3.4 (2018), p. 045005.
- [29] Ronan Gautier, Élie Genois, and Alexandre Blais. “Optimal Control in Large Open Quantum Systems: The Case of Transmon Readout and Reset”. Apr. 2024. arXiv: [2403.14765](https://arxiv.org/abs/2403.14765) [quant-ph]. (Visited on 07/29/2024).
- [30] Edward B Davies. “Quantum stochastic processes”. In: *Communications in Mathematical Physics* 15.4 (1969), pp. 277–304.
- [31] Howard Carmichael. *An Open Systems Approach to Quantum Optics: Lectures Presented at the Université Libre de Bruxelles October 28 to November 4, 1991*. en. Vol. 18. Lecture Notes in Physics Monographs. Berlin, Heidelberg: Springer, 1993. ISBN: 978-3-540-56634-2 978-3-540-47620-7. DOI: [10.1007/978-3-540-47620-7](https://doi.org/10.1007/978-3-540-47620-7). URL: <http://link.springer.com/10.1007/978-3-540-47620-7> (visited on 11/26/2023).
- [32] Ian Percival. *Quantum state diffusion*. Cambridge University Press, 1998.
- [33] Andrew J. Daley. “Quantum Trajectories and Open Many-Body Quantum Systems”. In: *Advances in Physics* 63.2 (2014), pp. 77–149. ISSN: 14606976. DOI: [10.1080/00018732.2014.933502](https://doi.org/10.1080/00018732.2014.933502). arXiv: [1405.6694](https://arxiv.org/abs/1405.6694).

- [34] K. W. Murch et al. “Observing single quantum trajectories of a superconducting quantum bit”. en. In: *Nature* 502.7470 (2013). Publisher: Nature Publishing Group, pp. 211–214. ISSN: 1476-4687. DOI: [10.1038/nature12539](https://doi.org/10.1038/nature12539). URL: <https://www.nature.com/articles/nature12539> (visited on 08/13/2024).
- [35] P. Campagne-Ibarcq et al. “Observing Quantum State Diffusion by Heterodyne Detection of Fluorescence”. In: *Physical Review X* 6.1 (2016). Publisher: American Physical Society, p. 011002. DOI: [10.1103/PhysRevX.6.011002](https://doi.org/10.1103/PhysRevX.6.011002). URL: <https://link.aps.org/doi/10.1103/PhysRevX.6.011002> (visited on 08/13/2024).
- [36] Q. Ficheux et al. “Dynamics of a qubit while simultaneously monitoring its relaxation and dephasing”. en. In: *Nature Communications* 9.1 (2018). Publisher: Nature Publishing Group, p. 1926. ISSN: 2041-1723. DOI: [10.1038/s41467-018-04372-9](https://doi.org/10.1038/s41467-018-04372-9). URL: <https://www.nature.com/articles/s41467-018-04372-9> (visited on 08/13/2024).
- [37] Z. K. Mineev et al. “To catch and reverse a quantum jump mid-flight”. en. In: *Nature* 570.7760 (2019). Publisher: Nature Publishing Group, pp. 200–204. ISSN: 1476-4687. DOI: [10.1038/s41586-019-1287-z](https://doi.org/10.1038/s41586-019-1287-z). URL: <https://www.nature.com/articles/s41586-019-1287-z> (visited on 08/13/2024).
- [38] Witłef Wieczorek et al. “Optimal State Estimation for Cavity Optomechanical Systems”. In: *Physical Review Letters* 114.22 (2015). Publisher: American Physical Society, p. 223601. DOI: [10.1103/PhysRevLett.114.223601](https://doi.org/10.1103/PhysRevLett.114.223601). URL: <https://link.aps.org/doi/10.1103/PhysRevLett.114.223601> (visited on 08/13/2024).
- [39] Massimiliano Rossi et al. “Observing and Verifying the Quantum Trajectory of a Mechanical Resonator”. en. In: *Physical Review Letters* 123.16 (2019), p. 163601. ISSN: 0031-9007, 1079-7114. DOI: [10.1103/PhysRevLett.123.163601](https://doi.org/10.1103/PhysRevLett.123.163601). URL: <https://link.aps.org/doi/10.1103/PhysRevLett.123.163601> (visited on 08/13/2024).
- [40] Rodrigo A. Thomas et al. “Entanglement between distant macroscopic mechanical and spin systems”. en. In: *Nature Physics* 17.2 (2021). Publisher: Nature Publishing Group, pp. 228–233. ISSN: 1745-2481. DOI: [10.1038/s41567-020-1031-5](https://doi.org/10.1038/s41567-020-1031-5). URL: <https://www.nature.com/articles/s41567-020-1031-5> (visited on 08/13/2024).
- [41] Mohamed Ragab Abdelhafez. “Quantum Optimal Control Using Automatic Differentiation”. PhD thesis. The University of Chicago, 2019.
- [42] Nicolas Gisin and Ian C Percival. “The quantum-state diffusion model applied to open systems”. In: *Journal of Physics A: Mathematical and General* 25.21 (1992), p. 5677.
- [43] Alberto Barchielli and Matteo Gregoratti. *Quantum Trajectories and Measurements in Continuous Time: The Diffusive Case*. Vol. 782. Lecture Notes in Physics. Berlin, Heidelberg: Springer Berlin Heidelberg, 2009. ISBN: 978-3-642-01297-6 978-3-642-01298-3. DOI: [10.1007/978-3-642-01298-3](https://doi.org/10.1007/978-3-642-01298-3). (Visited on 11/30/2023).
- [44] Howard M Wiseman and Gerard J Milburn. “Quantum theory of optical feedback via homodyne detection”. In: *Physical Review Letters* 70.5 (1993), p. 548.
- [45] VP Belavkin. “Theory of the control of observable quantum systems”. In: *Automatica and Remote Control* 44.2 (1983), pp. 178–188.
- [46] VP Belavkin, Osamu Hirota, and Robin Lyth Hudson. *Quantum communications and measurement*. Springer Science & Business Media, 2013.
- [47] Howard M Wiseman and Gerard J Milburn. *Quantum measurement and control*. Cambridge university press, 2009.
- [48] Huy en Pham. *Continuous-time stochastic control and optimization with financial applications*. Vol. 61. Springer Science & Business Media, 2009.

- [49] J Yong and X.Y. Zhou. *Stochastic controls. Hamiltonian Systems and HJB Equations*. Springer, 1999.
- [50] A. C. Doherty and K. Jacobs. “Feedback control of quantum systems using continuous state estimation”. en. In: *Physical Review A* 60.4 (1999), pp. 2700–2711. ISSN: 1050-2947, 1094-1622. DOI: [10.1103/PhysRevA.60.2700](https://doi.org/10.1103/PhysRevA.60.2700). URL: <https://link.aps.org/doi/10.1103/PhysRevA.60.2700> (visited on 07/23/2024).
- [51] Andrew C. Doherty et al. “Quantum Feedback Control and Classical Control Theory”. In: *Physical Review A - Atomic, Molecular, and Optical Physics* 62.1 (2000), p. 13. ISSN: 10941622. DOI: [10.1103/PhysRevA.62.012105](https://doi.org/10.1103/PhysRevA.62.012105). arXiv: [quant-ph/9912107](https://arxiv.org/abs/quant-ph/9912107).
- [52] H.J. Kappen. “Linear theory for control of non-linear stochastic systems”. In: *Physical Review letters* 95 (2005), p. 200201.
- [53] H.J. Kappen and H.C. Ruiz. “Adaptive importance sampling for control and inference”. In: *Journal of Statistical Physics* (2016), 10.1007/s10955–016–1446–7.
- [54] Sep Thijssen and H. J. Kappen. “Path integral control and state-dependent feedback”. In: *Phys. Rev. E* 91 (3 2015). <http://arxiv.org/abs/1406.4026>, p. 032104. DOI: [10.1103/PhysRevE.91.032104](https://doi.org/10.1103/PhysRevE.91.032104). URL: <http://link.aps.org/doi/10.1103/PhysRevE.91.032104>.
- [55] Grady Williams et al. “Aggressive driving with model predictive path integral control”. In: *Robotics and Automation (ICRA), 2016 IEEE International Conference on*. IEEE. 2016, pp. 1433–1440.
- [56] Muhammad Kazim et al. “Recent advances in path integral control for trajectory optimization: An overview in theoretical and algorithmic perspectives”. In: *Annual Reviews in Control* 57 (2024), p. 100931.
- [57] *AN OPTIMAL STOCHASTIC CONTROLLER FOR AN OPEN QUANTUM SYSTEM. European patent application EP24207671 submitted 20 October 2024.*
- [58] Heinz-Peter Breuer and Francesco Petruccione. *The theory of open quantum systems*. Oxford University Press, USA, 2002.
- [59] Brecht Donvil and Paolo Muratore-Ginanneschi. “Unraveling-paired dynamical maps recover the input of quantum channels”. In: *New Journal of Physics* 25.5 (2023), p. 053031.
- [60] H. M. Wiseman and L. Diósi. “Complete Parameterization, and Invariance, of Diffusive Quantum Trajectories for Markovian Open Systems”. In: *Chemical Physics* 268.1-3 (2001), pp. 91–104. ISSN: 03010104. DOI: [10.1016/S0301-0104\(01\)00296-8](https://doi.org/10.1016/S0301-0104(01)00296-8). arXiv: [quant-ph/0012016](https://arxiv.org/abs/quant-ph/0012016).
- [61] Robin L Hudson and Kalyanapuram R Parthasarathy. “Quantum Itô’s formula and stochastic evolutions”. In: *Communications in mathematical physics* 93 (1984), pp. 301–323.
- [62] Kalyanapuram R Parthasarathy. *An introduction to quantum stochastic calculus*. Vol. 85. Birkhäuser, 2012.
- [63] Alberto Barchielli and Viacheslav P Belavkin. “Measurements continuous in time and a posteriori states in quantum mechanics”. In: *Journal of Physics A: Mathematical and General* 24.7 (1991), p. 1495.
- [64] Lajos Diósi and Walter T Strunz. “The non-Markovian stochastic Schrödinger equation for open systems”. In: *Physics Letters A* 235.6 (1997), pp. 569–573.
- [65] Jay Gambetta and Howard M Wiseman. “Non-Markovian stochastic Schrödinger equations: Generalization to real-valued noise using quantum-measurement theory”. In: *Physical Review A* 66.1 (2002), p. 012108.
- [66] Alberto Barchielli and Matteo Gregoratti. *Quantum trajectories and measurements in continuous time: the diffusive case*. Vol. 782. Springer, 2009.

- [67] I Semina et al. “Stochastic Schrödinger equations for Markovian and non-Markovian cases”. In: *Open Systems & Information Dynamics* 21.01n02 (2014), p. 1440008.
- [68] Laurens Van der Maaten and Geoffrey Hinton. “Visualizing data using t-SNE.” In: *Journal of machine learning research* 9.11 (2008).
- [69] Lieven MK Vandersypen and Isaac L Chuang. “NMR techniques for quantum control and computation”. In: *Reviews of modern physics* 76.4 (2004), pp. 1037–1069.
- [70] Sonia G Schirmer, H Fu, and Allan I Solomon. “Complete controllability of quantum systems”. In: *Physical Review A* 63.6 (2001), p. 063410.
- [71] Jonathan A Jones, RH Hansen, and Michael Mosca. “Quantum logic gates and nuclear magnetic resonance pulse sequences”. In: *Journal of Magnetic Resonance* 135.2 (1998), pp. 353–360.
- [72] David A Meyer and Nolan R Wallach. “Global entanglement in multiparticle systems”. In: *Journal of Mathematical Physics* 43.9 (2002), pp. 4273–4278.
- [73] Yuquan Chen et al. “Accelerating quantum optimal control through iterative gradient-ascent pulse engineering”. In: *Physical Review A* 108.5 (2023), p. 052603.
- [74] Alicia B Magann et al. “From pulses to circuits and back again: A quantum optimal control perspective on variational quantum algorithms”. In: *PRX Quantum* 2.1 (2021), p. 010101.
- [75] Alexandre Choquette et al. “Quantum-optimal-control-inspired ansatz for variational quantum algorithms”. In: *Physical Review Research* 3.2 (2021), p. 023092.
- [76] Oinam Romesh Meitei et al. “Gate-free state preparation for fast variational quantum eigensolver simulations”. In: *npj Quantum Information* 7.1 (2021), p. 155.
- [77] Robert De Keijzer, Oliver Tse, and Servaas Kokkelmans. “Pulse based Variational Quantum Optimal Control for hybrid quantum computing”. In: *Quantum* 7 (2023), p. 908.
- [78] H. J. Kappen and H. C. Ruiz. “Adaptive Importance Sampling for Control and Inference”. In: *Journal of Statistical Physics* 162.5 (2016), pp. 1244–1266. ISSN: 00224715. DOI: [10.1007/s10955-016-1446-7](https://doi.org/10.1007/s10955-016-1446-7). arXiv: [1505.01874](https://arxiv.org/abs/1505.01874).
- [79] Michael Bartholomew-Biggs et al. “Automatic Differentiation of Algorithms”. In: *Journal of Computational and Applied Mathematics. Numerical Analysis 2000. Vol. IV: Optimization and Nonlinear Equations* 124.1 (Dec. 2000), pp. 171–190. ISSN: 0377-0427. DOI: [10.1016/S0377-0427\(00\)00422-2](https://doi.org/10.1016/S0377-0427(00)00422-2). (Visited on 08/29/2024).
- [80] Alain Bensoussan. *Stochastic control of partially observable systems*. Cambridge University Press, 1992.
- [81] Karl Kraus et al. *States, Effects, and Operations Fundamental Notions of Quantum Theory: Lectures in Mathematical Physics at the University of Texas at Austin*. Springer, 1983.
- [82] Yakir Aharonov, David Z. Albert, and Lev Vaidman. “How the result of a measurement of a component of the spin of a spin- $1/2$ particle can turn out to be 100”. en. In: *Physical Review Letters* 60.14 (1988), pp. 1351–1354. ISSN: 0031-9007. DOI: [10.1103/PhysRevLett.60.1351](https://doi.org/10.1103/PhysRevLett.60.1351). URL: <https://link.aps.org/doi/10.1103/PhysRevLett.60.1351> (visited on 07/16/2023).
- [83] Michael Hatridge et al. “Quantum back-action of an individual variable-strength measurement”. In: *Science* 339.6116 (2013), pp. 178–181.
- [84] H. J. Kappen. “Path Integrals and Symmetry Breaking for Optimal Control Theory”. In: *Journal of Statistical Mechanics: Theory and Experiment* 11 (2005), pp. 205–229. ISSN: 17425468. DOI: [10.1088/1742-5468/2005/11/P11011](https://doi.org/10.1088/1742-5468/2005/11/P11011). arXiv: [physics/0505066](https://arxiv.org/abs/physics/0505066).
- [85] Sep Thijssen and H. J. Kappen. “Path Integral Control and State-Dependent Feedback”. In: *Physical Review E - Statistical, Nonlinear, and Soft Matter Physics* 91.3 (2015). ISSN: 15502376. DOI: [10.1103/PhysRevE.91.032104](https://doi.org/10.1103/PhysRevE.91.032104). arXiv: [1406.4026](https://arxiv.org/abs/1406.4026).

- [86] Pierre Guilmin et al. “Dynamics: an open-source Python library for GPU-accelerated and differentiable simulation of quantum systems”. 2024. URL: <https://github.com/dynamics/dynamics>.
- [87] Marin Bukov et al. “Reinforcement Learning in Different Phases of Quantum Control”. In: *Physical Review X* 8.3 (2018). arXiv:1705.00565 [cond-mat, physics:quant-ph], p. 031086. ISSN: 2160-3308. DOI: [10.1103/PhysRevX.8.031086](https://doi.org/10.1103/PhysRevX.8.031086). URL: <http://arxiv.org/abs/1705.00565> (visited on 11/26/2023).

Supplementary Material

We provide with the supplementary material for the paper "Quantum optimal control via path integrals" containing proofs and additional numerical experiments.

1 Unraveling calculations

Proof of Proposition (1) in the paper.

Proof.

$$d\psi = -iH'\psi dt - \frac{1}{2}D_{ab}C_b^\dagger C'_a\psi dt + C'_a\psi dW^a \quad (32)$$

with $\langle dW_a dW_b \rangle = D_{ab}dt$ and H', C' to be defined later. Define the quantum state $P = \psi\psi^\dagger$. Then using Ito calculus, the dynamics of P is

$$dP = d\psi\psi^\dagger + \psi d\psi^\dagger + d\psi d\psi^\dagger = -i[H', P]dt + \mathcal{D}[C', D](P)dt + [C'_a P dW_a + \text{h.c.}] \quad (33)$$

ψ is a stochastic vector with norm $\|\psi\|^2 = \psi^\dagger\psi$. Using Ito calculus, the change in the norm is given by

$$d(\|\psi\|^2) = d\psi^\dagger\psi + \psi^\dagger d\psi + d\psi^\dagger d\psi = \psi^\dagger(C'_a + (C'_a)^\dagger)\psi dW_a \quad (34)$$

We can ensure that $\|\psi\|^2$ is conserved by defining $C'_a = C_a - c_a$ with $c_a = \psi^\dagger C_a^{(h)}\psi$ and $C_a^{(h)}$ the Hermitian part of C_a . Note, that c_a is real. With this choice Eqs. (32) and (33) become ⁵

$$d\psi = -iH'\psi dt - \frac{1}{2}D_{ab}(C_b - c_b)^\dagger(C_a - c_a)\psi dt + (C_a - c_a)\psi dW_a \quad (35)$$

$$dP = -i[H' - iD_{ab}c_a C_b^{(ah)}, P] + \mathcal{D}[C, D](P)dt + [(C_a - c_a)P dW_a + \text{h.c.}] \quad (36)$$

with $C_a^{(ah)} = \frac{1}{2}(C_a - C_a^\dagger)$. To connect to the Lindblad equation, define $H = H' - iD_{ab}c_a C_b^{(ah)}$. Then substitution in (35) and (36) yields

$$d\psi = -iH\psi dt - \frac{1}{2}D_{ab}\left(C_b^\dagger C_a - 2c_a C_b + c_a c_b\right)\psi dt + (C_a - c_a)\psi dW_a \quad (37)$$

and

$$dP = -i[H, P]dt + \mathcal{D}[C, D](P)dt + [(C_a - c_a)P dW_a + \text{h.c.}] \quad (38)$$

Define $\rho := \langle P \rangle$ and $\langle dP \rangle := \dot{\rho}dt$. Taking the average of (38) yields the Lindblad equation

$$\dot{\rho} = -i[H, \rho] + \mathcal{D}[D, C]\rho \quad \mathcal{D}[D, C]\rho := D_{ab}\left(C_a\rho C_b^\dagger - \frac{1}{2}\{C_b^\dagger C_a, \rho\}\right) \quad (39)$$

which completes the proof. □

⁵

$$\begin{aligned} \mathcal{D}[C', D'](P) &= D_{ab}\left((C_a - c_a)P(C_b - c_b)^\dagger - \frac{1}{2}\{(C_b - c_b)^\dagger(C_a - c_a), P\}\right) \\ &= \mathcal{D}[C, D](P) + \frac{1}{2}D_{ab}c_a[C_b^\dagger, P] - \frac{1}{2}D_{ab}c_a[C_b, P] \\ &= \mathcal{D}[C, D](P) - D_{ab}c_a[C_b^{(ah)}, P] = \mathcal{D}[C, D](P) - i[-iD_{kl}c_k C_l^{(ah)}, P] \end{aligned}$$

2 Path integral control theory

In this section we describe some basic results regarding PI control theory. For further details the reader may consult the original papers [84, 85].

Define

$$\psi(t, x) = e^{-J(t,x)/\lambda} \quad \phi(t) = e^{(S^u(t) - S^u(t_0))/\lambda}$$

where $\lambda I = R\nu$. Furthermore we define the stochastic processes $\psi(t) = \psi(t, X_t^u)$, $u(t) = u(t, X_t^u)$ and $u^*(t) = u^*(t, X_t^u)$

Lemma 1. For all t in $t_0 \leq t \leq t_1$

$$e^{-S^u(t)/\lambda} - \psi(t) = \frac{1}{\lambda\phi(t)} \int_t^{t_1} \phi(s)\psi(s)(u^*(s) - u(s))^T RdW_s \quad (40)$$

Proof. Define the optimal cost-to-go as the minimal expected cost starting in any x at time t with $t_0 \leq t \leq t_1$

$$J(t, x) = \min_u \langle S^u(t) \rangle_{X_t^u=x} \quad u^*(t, x) = \operatorname{argmin}_u \langle S^u(t) \rangle_{X_t^u=x} \quad (41)$$

where the minimization is over all smooth functions $u(\cdot, s)$, $t \leq s \leq t_1$. The HJB equation for the control problem Eqs. (6) and (7) in the paper is

$$-J_t = \min_u \left(V + \frac{1}{2}u^T R u + (f + gu)^T J_x + \frac{1}{2}\operatorname{Tr}(g\nu g^T J_{xx}) \right)$$

where subscripts t, x denote differentiation with respect to t, x and with boundary condition $J(t_1, x) = \Phi(x)$. We can solve for u , which gives $u^* = -R^{-1}g^T J_x$ and

$$-J_t = V - \frac{1}{2}J_x^T g R^{-1} g^T J_x + f^T J_x + \frac{1}{2}\operatorname{Tr}(g\nu g^T J_{xx}) \quad (42)$$

We assume that the matrices R, ν are related such that $R = \lambda\nu^{-1}$ with $\lambda > 0$. In terms of ψ , Eq. (42) becomes linear

$$\psi_t + f^T \psi_x + \frac{1}{2}\operatorname{Tr}(g\nu g^T \psi_{xx}) = \frac{V}{\lambda} \psi \quad (43)$$

Alternatively, we consider the stochastic process $\psi(t) = \psi(t, X_t^u)$. Using \hat{I} to calculus we obtain

$$d\psi = \left(\psi_t + \psi_x^T (f + gu) + \frac{1}{2}\operatorname{Tr}(g\nu g^T \psi_{xx}) \right) dt + \psi_x^T g dW = \frac{V}{\lambda} \psi + \psi_x^T g (udt + dW)$$

where we used Eq. (43), with boundary condition $\psi(t_1, x) = e^{-\Phi(x)/\lambda}$. Using the definition of $\phi(t)$ we obtain

$$d\phi = -\frac{1}{\lambda} \left(V dt + u^T RdW \right)$$

with initial condition $\phi(t_0) = 1$. Using the product rule we obtain

$$d(\phi\psi) = d\phi\psi + \phi d\psi + d[\phi, \psi] = -\frac{1}{\lambda}\phi\psi u^T RdW + \phi\psi_x^T g dW = \frac{1}{\lambda}\phi\psi(u^* - u)^T RdW$$

where in the last step we used $u^* = \lambda R^{-1}g^T \frac{\psi_x}{\psi}$. Integrating from t to t_1 we obtain

$$\phi(t_1)\psi(t_1) - \phi(t)\psi(t) = \frac{1}{\lambda} \int_t^{t_1} \phi(s)\psi(s)(u^*(s) - u(s))^T RdW_s$$

We use $\phi(t_1) = \phi(t)e^{(S^u(t_1) - S^u(t))/\lambda}$ and divide by $\phi(t)$ to obtain Eq. (40). \square

Corollary 2. We take the expectation of Eq. (40) with respect to $dW_{t:t_1}$ and condition on events up to time t , which we call a filtration \mathcal{F}_t , we obtain

$$\psi(t) = \left\langle e^{-S^u(t)/\lambda} \right\rangle_{\mathcal{F}_t} \quad (44)$$

The following path integral control theorem is useful to estimate these parameters for all times from one set of samples $X_{t_0:t_1}^u$.

Theorem 3. Let $f : \mathbb{R} \times \mathbb{R}^n \rightarrow \mathbb{R}$ and define the process $f_t = f(t, X_t^u)$. Then

$$\left\langle e^{-S^u(t_0)/\lambda} \int_{t_0}^{t_1} (u^*(s) - u(s))f(s)ds \right\rangle = \left\langle e^{-S^u(t_0)/\lambda} \int_{t_0}^{t_1} f(s)dW_s \right\rangle \quad (45)$$

where the expectation is with respect to the stochastic process (6) in the paper.

Proof. Consider Lemma (1) for $t = t_0$. Multiply both sides by $\int_{t_0}^{t_1} f(s)dW_s$ and take the expectation value

$$\left\langle e^{-S^u(t_0)} \int_{t_0}^{t_1} f(s)dW_s \right\rangle = \left\langle \int_{t_0}^{t_1} f(s)dW_s \int_{t_0}^{t_1} \phi(s')\psi(s')(u^*(s') - u(s'))^T \frac{R}{\lambda} dW_{s'} \right\rangle \quad (46)$$

Using $RD = \lambda$ and Ito isometry we have

$$\left\langle e^{-S^u(t_0)} \int_{t_0}^{t_1} f(s)dW_s \right\rangle = \int_{t_0}^{t_1} \langle f(s)\phi(s)\psi(s)(u^*(s) - u(s)) \rangle ds \quad (47)$$

Using the definition of $\psi(s)$ and $\phi(s)$ we write

$$\left\langle e^{-S^u(t_0)} \int_{t_0}^{t_1} f(s)dW_s \right\rangle = \int_{t_0}^{t_1} \left\langle f(s)e^{(S^u(s)-S^u(t_0))/\lambda} \left\langle e^{-S^u(t_0)} \right\rangle_{\mathcal{F}_s} (u^*(s) - u(s)) \right\rangle ds \quad (48)$$

Finally, by applying the law of total expectation we obtain (45). □

Corollary 4. By setting $f(t) = \delta_{t \in I}$ with $I = [t_0, t_0 + dt]$, diving by dt and taking the limit $dt \rightarrow 0$ we establish the proof of (9) in the paper.

3 Open GRAPE

Here we summarize the details of our implementation of Open GRAPE for the benchmarking part of Section 6.1 in the paper. For further details concerning the definition of Open GRAPE algorithm we refer the reader to [27]. Given the cost objective (18) and the control model Eq. (12) in the paper, with R a positive scalar, the first order Open GRAPE update rule (ignoring terms of $\mathcal{O}(dt^2)$ and higher) becomes

$$A_{ak} \rightarrow A'_{ak} = A_{ak} - \varepsilon \frac{\partial C}{\partial A_{ak}}$$

with

$$\frac{\partial C}{\partial A_{ak}} = \frac{iQ}{2} \text{Tr}(\lambda_k[H_a, \rho_k]) dt + RA_{ak}dt$$

where ρ_k is the forward-propagated state from ρ_0 to time t_k and λ_k is the backward-propagated state from ρ_{target} to time t_k , ε is the learning rate, and dt is the time step. We implement the algorithm in Python language. For the dynamics simulation of the backward and forward propagations we use the open-source Python package `dynamics` [86].

The learning rate ε usually needs to be carefully chosen in order to avoid overshooting. In the case of GRAPE for closed systems, work [87] reported an adaptive learning rate at each j step of ε/j^α with $\alpha = 1/2$ was enough to avoid overshooting of local minima/saddle points. We found this approach not suitable for our benchmarking purposes as it required an excessive fine tuning of α for different types of seeds. We choose instead the following protocol: every time the cost $C(A') \geq C(A)$, where A the current solution and A' the new solution, the learning rate is reduced by a factor 10 and $C(A')$ is recomputed until either $C(A') < C(A)$ or ε is reduced a maximum number of times that we set to 10. This stopping condition allows us to capture local minima and detect when the first order approximation of the gradient update starts to fail. At the start of each run, we sample random seeds u from Gaussian distributions (centered at zero, 1, and -1, with standard deviation 2) and uniform distributions (integers between -10 and 10, with a scale factor of 1 and 0.5).

4 Open NMR control theory

4.1 Rotating frame transformation

Define the unitary transformation

$$U = \exp(iH_Z t) \quad H_Z = \pi \sum_j \nu_j \sigma_j^z \quad (49)$$

It represents a transformation from the lab frame to a multiple rotating frame. Given the state ρ in the lab frame, define the transformed state to the rotating frame by $\rho' = U\rho U^\dagger$. Assume ρ follows the generic Lindblad equation

$$\dot{\rho} = -i[H_Z + H_I + H_c, \rho] + \mathcal{D}[D, J]\rho \quad (50)$$

where, for simplicity, D is a real scalar and the J_a are arbitrary dissipators.

Lemma 2. *The transformed state ρ' follows the Lindblad equation*

$$\dot{\rho}' = -i[H_I + H'_c, \rho'] + \mathcal{D}[D, J']\rho' \quad (51)$$

where

$$H'_c = \sum_i u'_{ix} \sigma_i^x + u'_{iy} \sigma_i^y \quad J'_a = U J_a U^\dagger \quad (52)$$

and the controls in the rotating frame, $u'_i = (u'_{ix}, u'_{iy})^T$, are related to those in the lab frame, $u_i = (u_{ix}, u_{iy})^T$, by a real rotation

$$u'_i = S_i(t) u_i \quad S_i(t) = \begin{pmatrix} \cos(2\pi\nu_i t) & \sin(2\pi\nu_i t) \\ -\sin(2\pi\nu_i t) & \cos(2\pi\nu_i t) \end{pmatrix} \quad (53)$$

Proof. By differentiating ρ' w.r.t. time we obtain

$$\begin{aligned} \dot{\rho}' &= \dot{U} \rho U^\dagger + U \dot{\rho} U^\dagger + U \rho \dot{U}^\dagger \\ &= -i[H_I + H'_c, \rho'] + \mathcal{D}[D, J']\rho' \end{aligned}$$

where $H'_c = U H_c U^\dagger$ and $J'_a = U J_a U^\dagger$.

Next, compute

$$H'_c = U H_c U^\dagger = \sum_i u_{ix} (U \sigma_i^x U^\dagger + u_{iy} U \sigma_i^y U^\dagger)$$

For each spin i we obtain

$$\begin{aligned} U\sigma_i^x U^\dagger &= e^{i\pi\nu_i t \sigma_i^z} \sigma_i^x e^{-i\pi\nu_i t \sigma_i^z} \\ &= \cos(2\pi\nu_i t) \sigma_i^x - \sin(2\pi\nu_i t) \sigma_i^y \end{aligned}$$

and

$$\begin{aligned} U\sigma_i^y U^\dagger &= e^{i\pi\nu_i t \sigma_i^z} \sigma_i^y e^{-i\pi\nu_i t \sigma_i^z} \\ &= \cos(2\pi\nu_i t) \sigma_i^y + \sin(2\pi\nu_i t) \sigma_i^x \end{aligned}$$

Then, we can write H'_c as

$$H'_c = \sum_i u'_{ix} \sigma_i^x + u'_{iy} \sigma_i^y$$

where

$$\begin{aligned} u'_{ix} &= \cos(2\pi\nu_i t) u_{ix} + \sin(2\pi\nu_i t) u_{iy} \\ u'_{iy} &= -\sin(2\pi\nu_i t) u_{ix} + \cos(2\pi\nu_i t) u_{iy} \end{aligned} \quad (54)$$

By defining

$$S_i(t) = \begin{pmatrix} \cos(2\pi\nu_i t) & \sin(2\pi\nu_i t) \\ -\sin(2\pi\nu_i t) & \cos(2\pi\nu_i t) \end{pmatrix}, \quad (55)$$

$u'_i = (u'_{ix}, u'_{iy})^T$ and $u_i = (u_{ix}, u_{iy})^T$, we rewrite (54) as $u'_i = S_i(t)u_i$ and the Lemma is proved. \square

Assume the NMR system is in interaction with a EM field bath, which we encode in the dissipators $C_a = \sigma_i^+, \sigma_i^-$ ($i = 1, \dots, n$).

Lemma 3. *The dissipator in (50) is invariant under the action of U , i.e. $\mathcal{D}[D, C'] = \mathcal{D}[D, C]$.*

Proof. Apply the unitary transformation U to the Lindblad operators.

$$\begin{aligned} U\sigma_i^+ U^\dagger &= e^{i\pi\nu_i t \sigma_i^z} \sigma_i^+ e^{-i\pi\nu_i t \sigma_i^z} \\ &= e^{i2\pi\nu_i t} \sigma_i^+ \end{aligned}$$

where we used that $[\sigma_i^z, \sigma_i^+] = 2\sigma_i^+$. Analogously for σ_i^- , we have $U\sigma_i^- U^\dagger = e^{-i2\pi\nu_i t} \sigma_i^-$. Therefore, the Lindblad operators C'_a in the rotating frame are the same as in the lab frame up to phase factors. As the dissipator is invariant under phase transformations, the Lemma is thus proven. \square

4.2 Control problem equivalence

The main purpose of the unitary transformation U is to factor out potentially fast frequencies ν from the definition of the control problem that are not necessary for computing the optimal control and may even hinder the efficient search for a solution. By defining and solving the control problem in the rotating frame, we can uniquely map the optimal solution back to the lab frame through the action of the unitary transformation in control space. In this Section we describe a general invariance present in the control problem under certain family of transformations \mathcal{T} .

Assume the Lindblad equation for an open NMR system

$$\dot{\rho} = -i[H, \rho] + \mathcal{D}[D, C]\rho \quad (56)$$

with $H = H_Z + H_I + H_c$ and dissipator

$$\mathcal{D}[D, C]\rho = \sum_j D_{jab} \left(C_{ja}\rho C_{jb}^\dagger - \frac{1}{2}\{C_{jb}^\dagger C_{ja}, \rho\} \right).$$

where index j labels qubit j , and the dissipation operators C_{ja} act on qubit j . The noise matrix D is in block diagonal form $D := \bigoplus_j D_j$ with $(D_j)_{ab} = D_{jab}$.

Define the cost

$$C[x] = -\frac{Q}{2}\text{Tr}(\rho_T \rho_{tar}) + \frac{1}{2} \sum_j \int_0^T u_j^T R_j u_j dt \quad (57)$$

where the tuple $x := (\rho_T, \rho_{tar}, u, R)$ with $R := \bigoplus_j R_j$ block diagonal.

Consider U as in Section 4.1 in the paper, and define the transformation $\mathcal{T} = (U, S)$ to the rotating frame by it's action on pair (ρ, u) , with $u = u_i (i = 1, \dots, n)$, as $\mathcal{T}(\rho, u) = (U\rho U^\dagger, Su)$, and it's action on pair (D, R) as $\mathcal{T}(D, R) = (S^T D S, S^T R S)$.

Under \mathcal{T} , the dissipators C_{ja} transform as

$$U C_{ja} U^\dagger = e^{i\alpha_j} \sum_b S_{jab} C_{jb} \quad (58)$$

where $S_j (j = 1, \dots, n)$ is an orthogonal matrix with $S_j S_j^T = 1$, α_j arbitrary real numbers, and define $S = \bigoplus_j S_j$.

Lemma 4. *The dissipator $\mathcal{D}[D, C]$ is invariant under \mathcal{T} , i.e. $\mathcal{D}[D', C'] = \mathcal{D}[D, C]$.*

Proof. The results follows by applying $\mathcal{T}D = SDS^T$ and definition (58) to the dissipators C_{ja} . \square

Theorem 5. *The cost $C[x]$ in (57) is invariant under \mathcal{T} and the optimal control solutions u'^* and u^* in the rotating and lab frames, respectively, are related by $u'^* = Su^*$.*

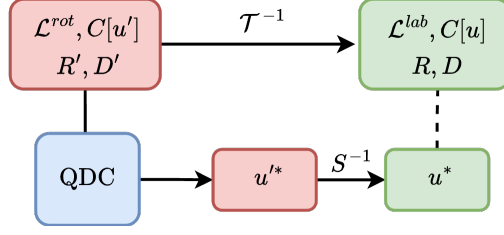
Proof. Write the action of \mathcal{T} on C as

$$\begin{aligned} (\mathcal{T}C)[x] &= C[\mathcal{T}x] \\ &= -\frac{Q}{2}\text{Tr}(\rho'_T \rho'_{tar}) + \frac{1}{2} \sum_j \int_0^T u_j'^T R_j' u_j' dt \\ &= -\frac{Q}{2}\text{Tr}(U\rho_T U^\dagger U\rho_{tar} U^\dagger) + \frac{1}{2} \sum_j \int_0^T (Su_j)^T S R_j S^T (Su_j) dt \\ &= C[x] \end{aligned}$$

where in the last line we used the unitarity/orthogonality of U and S_i , respectively. Thus, $C[x] = C[x']$ and the invariance of C follows.

Next, fix ρ_{tar} and R , and consider the optimal solution in the lab frame $u^* = \text{argmin}_u C[u]$, which satisfies $C[u^*] \leq C[u] \forall u$. By invariance of C under \mathcal{T} , and given that \mathcal{T} is invertible, the transformation Su^* satisfies $C[Su^*] \leq C[u'] \forall u'$ where $u' = Su$. Thus, the optimal solution in the rotating frame u'^* corresponds to a rotation of the optimal solution in the lab frame, $u'^* = Su^*$. \square

Provided that the dissipators C' in the rotating frame can be transformed to anti-Hermitian operators, we can solve the control problem in the rotating frame using the QDC algorithm. By virtue of Theorem 5, The optimal control u'^* in the rotating frame can be mapped back to the lab frame. Define \mathcal{L}^{rot} , \mathcal{L}^{lab} as the Lindbladian operators in the rotating and lab frames, respectively. The following diagram illustrates the end-to-end workflow of the transformation.



Example 1. A particular example of \mathcal{T} is the case in which the dissipators $C_a = \sigma_i^+, \sigma_i^-$. Then, S corresponds to the rotation defined in (53) and we can use the transformation A defined in (23) to transform to anti-hermitian operators and simulate the problem using QDC.

Example 2. When the target state in the lab frame is a GHZ state, i.e. $\phi = |GHZ\rangle$, the corresponding state in the rotating frame becomes $\phi' = U_T |GHZ\rangle = \frac{1}{\sqrt{2}}(e^{i2\pi\omega T} |0\rangle^n + e^{-i2\pi\omega T} |1\rangle^n)$ with $\omega = \frac{1}{2} \sum_j \nu_j$. In particular, note that $\phi' = \phi$ whenever $\omega T \in \mathbb{Z}$.

5 A 10 qubits example

Here we provide a complimentary example applying QDC to a 10-qubit toy model example to test the scalability of our algorithm.

Consider a 1-D spin chain of n qubits with single and pair-wise controls. Since this is a toy model designed to test the scalability of our algorithm for a larger number of qubits, we do not assert its feasibility in a lab setting, but rather emphasize the simplicity of defining such control problems within our framework. For simplicity, we set $H_0 = 0$. The control Hamiltonian is

$$H_c = \sum_{i=1}^n \sum_{a=x,y} u_{ia} \sigma_i^a + \sum_{i=1}^{n-1} \sum_{a,b=x,y} u_{iab} \sigma_i^a \sigma_{i+1}^b \quad (59)$$

where the controls u_{ia} act on spin i , and controls u_{iab} on the pair $i, i+1$. Note, that H_c is an extension of typical NMR control Hamiltonians [69] with the addition of pair-wise controls.

The open dynamics is described by the Lindblad equation

$$\dot{\rho} = -i[H, \rho] + D_1 \sum_{i=1}^n (\sigma_i^- \rho \sigma_i^+ + \sigma_i^+ \rho \sigma_i^- - \rho) + D_2 \sum_{i=1}^{n-1} \sum_{v,w=\pm} (\sigma_i^v \sigma_{i+1}^w \rho \sigma_i^{-v} \sigma_{i+1}^{-w} - \rho) \quad (60)$$

with dissipation σ^\pm of equal strength D_1 acting on individual spins and with strength D_2 on neighboring pairs of spins.

The control cost is defined as

$$C = \left\langle -\frac{Q}{2} \mathcal{F}(\psi_T) + \frac{1}{2} \int_0^T \left(R_1 \sum_{i=1}^n \sum_{a=x,y} u_{ia}^2 + R_2 \sum_{i=1}^{n-1} \sum_{a,b=x,y} u_{iab}^2 \right) dt \right\rangle \quad (61)$$

Analogous to the previous section, we perform the transformation (23) to map non-Hermitian operators into anti-Hermitian. We transform the operators $C_{ia} = \sigma_i^a, a = \pm$ and $C_{iab} = \sigma_i^a \sigma_{i+1}^b, a, b = \pm$ in Eq. (60) into anti-Hermitian operators

$$\tilde{C}_{ib} = C_{ia} A_{ab} \quad \tilde{C}_{icd} = C_{iab} A_{abcd} \quad \text{for all } i \quad (62)$$

with $A_{abcd} := iA_{ac}A_{bd}$. This leads to the following expression for the transformed operators

$$\tilde{C}_{ib} = -i\sigma_i^b \quad \tilde{C}_{icd} = -i\sigma_i^c \sigma_{i+1}^d \quad \text{for all } i \text{ and } b, c, d = x, y. \quad (63)$$

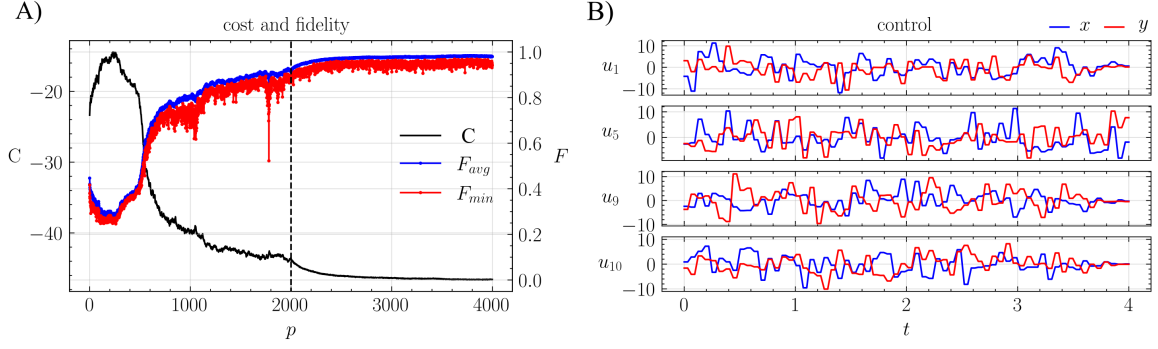


Figure 7: Control of a $n = 10$ qubit 1-D spin chain. The IS training (panel A) has two parts (marked by the vertical dashed line), where in the first part we set the IS window $w = 1$ (no smoothing), and in the second part we change it to $w = 10$. This is to speedup convergence in the first part, and later to improve the statistics. The average fidelity reached $F_{avg} = 0.982 \pm 0.001$. Runtime ~ 6.8 hr on a desktop computer. In panel (B) we illustrate the control solutions for qubits 1, 5, 9 and 10. The x/y components of each control are marked by blue and red colors, respectively. The parameters are $K = 64$, $T = 4$, $R=0.1$, $D = 0.001$, $Q=100$, $n_{IS}=4000$, and $N_{traj}=100$.

and $\tilde{D}_1 = \frac{1}{2}D_1$, $\tilde{D}_2 = \frac{1}{4}D_2$.

The corresponding unraveling is

$$d\psi = -i \left(\sum_{i=1}^n \sum_{a=x,y} (u_{ia}dt + d\tilde{W}_{ia})\sigma_i^a + \sum_{i=1}^{n-1} \sum_{a,b=x,y} (u_{iab}dt + d\tilde{W}_{iab})\sigma_i^a\sigma_{i+1}^b \right) \psi dt - (n\tilde{D}_1 + 2(n-1)\tilde{D}_2) \psi dt \quad (64)$$

with $\langle d\tilde{W}_{ia}d\tilde{W}_{jb} \rangle = \delta_{ij}\delta_{ab}\tilde{D}_1dt$ for $i, j = 1, \dots, n$ and $a, b = x, y$, and $\langle d\tilde{W}_{iab}d\tilde{W}_{jcd} \rangle = \delta_{ij}\delta_{ac}\delta_{bd}\tilde{D}_2dt$ for $i, j = 1, \dots, n-1$ and $a, b, c, d = x, y$. Equations (61) and (64) define a path integral control problem when

$$\lambda = \tilde{D}_1R_1 = \tilde{D}_2R_2 \quad (65)$$

The initial state is $\psi_0 = |0\rangle^n$. We choose the target state ϕ to be a Greenberger–Horne–Zeilinger (GHZ) state, which is defined as $|GHZ_n\rangle := \frac{1}{\sqrt{2}}(|0\rangle^n + |1\rangle^n)$ for n -qubit systems and it represents a maximally entangled state in the global entanglement (or Meyer–Wallach) measure for multipartite systems [72]. We set $R_1 = R_2 = R/n_c$ with $n_c = 2n + 4(n-1)$ the total number of controls. This normalization defines a fluence cost per unit control. The PI condition (65) then implies that $\tilde{D}_2 = \tilde{D}_1$ or $D_2 = 2D_1$. We take as free parameters R and D_1 . We run the algorithm for $n = 10$ qubits. The results are presented in Fig. 7, highlighting the potential of QDC for controlling large quantum systems. It is worth noting that a direct implementation of this problem using Open GRAPE would necessitate the computation and storage of matrix exponentials of dimensions $N^2 \times N^2$ at each step K , which could become prohibitive in terms of memory requirements. This challenge underscores the need for an efficient implementation of the algorithm (see, for instance, [27, 41]) and/or the use of specialized software. In contrast, our QDC algorithm runs efficiently on a standard desktop computer.